Shanghai Jiao Tong University

University of Michigan- Shanghai Jiao Tong University Joint Institute

Capacity Analysis of Full Duplex Wireless Networks Via Stochastic Geometry

by

Huaiyu Huang

A thesis submitted in satisfaction of the

requirements for the degree of Master of Science in

Electrical and Computer Engineering at Shanghai Jiao Tong University

Committee in charge: Shanghai

Prof. Xudong Wang, Chair   March, 2014

Prof. Xinen Zhu

Prof. Weikang Qian

Abstract

Recently, full duplex wireless communication is realized by advanced physical-layer techniques, thus, a radio can transmit and receive signals on the same frequency simultaneously. Compared with half duplex communication, the network throughput can be doubled in a single hop wireless network. However, it is still an open research topic on throughput gains from full duplex communications in large scale wireless networks. To solve this problem, we employed tools from stochastic geometry to analyze network capacity in two types of wireless networks, ad hoc networks and cellular networks.

As for ad hoc networks, the network topology is modeled as a Poisson cluster point process and the aggregate interference is calculated using a shot-noise process. To measure the network capacity, the notion of transmission capacity is utilized, which is the maximum successful transmission throughput in a unit area, subjecting to a constraint on outage probability. Based on our proposed model, performances of both half and full duplex wireless networks under three communication scenarios are presented. Firstly, transmission throughput is plotted for the same network density and transmission rate requirements. Results indicate that full duplex communication outperforms half duplex communication in the low transmission rate region and half duplex communication outperforms full duplex communication in the high transmission rate region. Secondly, under the same network density and the same outage requirement, transmission capacity, i.e. maximum transmission throughput, is presented by increasing the transmission rate. The results are consistent with transmission throughput in the first case. At last, fixed transmission rate and outage requirement are set to be the same for half duplex and full duplex wireless networks. Transmission capacity by maximizing network density is given. Results show that full duplex transmission capacity is always larger than half duplex transmission capacity, indicating that full duplex communication outperforms half duplex communication via more concurrent transmission opportunities.

As for cellular networks, assume full duplex radios installed on base stations, and a new technique mutual interference cancelation (MIC) is put forward to combat mutual interference between transmission pairs. Perfect MIC is defined and implemented on base stations for full duplex cellular network. The Network topology is modeled as two-layer Poisson point process with two identical density for each layer and the aggregate interference is analyzed following shot-noise process. Coverage probability and average rate of a typical uplink and downlink are derived. Comparisons of coverage probability and average rate are conducted between

half duplex communications and full duplex communications with/without MIC. Numerical results are run in two scenarios, zero background noise and nonzero background noise. In the zero background noise scenario, coverage probability is expressed in closed-form, and it is independent with network density. Thus, network capacity gain of full duplex communication is independent with network density when noise is neglected. In the nonzero noise background scenario, the coverage probability is expressed by closed-form related to Q-function, the tail probability of the standard normal distribution, when path-loss parameter is 4. The numerical results show that network capacity gain of full duplex communication degrades when network density is increased, which is consistent with the situation in wireless ad hoc network. Moreover, the network capacity gain also degrades when signal to noise ratio (SNR) increases, and is improved significantly when adopting MIC at the base stations. Thus, network capacity gain from full duplex communication is very limited and MIC can improve the network capacity gain significantly.

上海交通大学

交大密西根学院

基于随机几何的全双工无线网络容量分析

黄怀玉

上海交通大学密西根学院硕士学位论文

电子科学与技术专业

委员会成员：

王旭东（主席）

朱欣恩

钱炜慷

上海

2014 年 3 月

上海交通大学

学位论文原创性声明

本人郑重声明：所呈交的学位论文，是本人在导师的指导下，独立进行研究工作所取得的成果。除文中已经注明引用的内容外，本论文不包含任何其他个人或集体已经发表或撰写过的作品成果。对本文的研究做出重要贡献的个人和集体，均已在文中以明确方式标明。本人完全意识到本声明的法律结果由本人承担。

学位论文作者签名：黄小怀玉

日期：2014 年 3 月 1 日

附件五

上海交通大学
学位论文版权使用授权书

学位论文作者签名：黄怀玉　　　　指导教师签名：

日期：2014年 3 月 1 日　　　　日期：2014年 3 月 1 日

2

上海交通大学硕士学位论文答辩决议书
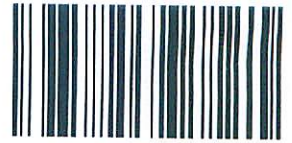
1113709011

姓　名	黄怀玉	学号	1113709011	所在学科	电子科学与技术		
指导教师	王旭东	答辩日期	2014-01-16	答辩地点	法学北楼二楼电阅		
论文题目			基于随机几何的全双工无线网络容量分析				

投票表决结果：**3/3/3**（同意票数/实到委员数/应到委员数）　答辩结论：☑通过　□未通过

评语和决议：

该论文首次分析了无线全双工通信网络的增

近容量。工作认真扎实。

黄怀玉认真准备了论文答辩，能够较好

地回答委员会提出的问题。委员会一致同

意黄怀玉通过论文答辩。

2014 年 1 月 17 日

答辩委员会成员签名	职务	姓名	职称	单位	签名
	主席	王旭东	副教授	上海交通大学	王旭东
	委员	钱炜慷	讲师	上海交通大学	钱炜慷
	委员	朱欣恩	讲师	上海交通大学	朱欣恩
	秘书	齐航	未评职称（高校教师）	上海交通大学	齐航

摘要

近来，先进的物理层技术实现了无线全双工通信，因此，无线终端可以在同一个频段上同时发送和接收信号。与半双工无线通信技术相比，无线全双工技术可以使单跳网络的网络吞吐量加倍。但是在大规模无线网络中，由无线全双工通信技术带来的网络容量增益仍然是一个未解的开发课题。为了解决这个课题，我们采用随机几何工具，分析无线自组织网络和蜂窝网络两种无线网络中网络容量增益。

针对自组织网络，其网络拓扑建模成一个泊松簇生点过程，网络聚集干扰采用 shot-noise 过程建模计算。使用传输容量概念来衡量最大网络吞吐量，即在限制中断概率情况下，单位面积内网络最大的成功传输吞吐量。基于我们建立的模型，给出了在三种通信场景下半双工和全双工网络的性能分析。首先，在相同节点密度和传输速率要求的情况下，我们绘制了传输吞吐量曲线。结果表明，在低传输速率区间，全双工通信优于半双工通信；在高传输速率区间，半双工通信优于全双工通信。其次，在相同网络节点密度和中断概率要求情况下，给出了最大传输吞吐量，即传输容量，与传输速率的关系曲线图。结果与第一中通信场景一致。最后，对于半双工和全双工无线网络，设定相同的固定传输速率和中断概率要求，给出了通过最大化网络节点密度而求得的传输容量。结果表明，全双工网络传输容量始终大于半双工网络容量。证明，与半双工通信相比，全双工通信的优势是通过创造更多的传输机会实现。

针对蜂窝网络，假设全双工天线安装在基站上，同时，提出了针对抵消传输对之间互干扰的互干扰消除技术。定义了理想互干扰消除技术并假设其在全双工蜂窝网络中的基站上实现。网络拓扑建模成相同点密度的双层泊松点过程，而网络聚集干扰使用 shot-noise 过程来分析。推导了典型上行和下行链路的覆盖概率和平均速率。针对半双工无线网络，以及使用或未使用互干扰消除技术的全双工无线网络，比较了三种网络的覆盖概率和平均速率。在零噪音及非零噪声两种场景下运行数值仿真。在零噪声场景中，可以给出闭式表达式来描述覆盖概率，而且其表达式与网络节点密度无关。因此，在零噪声场景情况下，全双工通信技术的网络容量增益与网络节点密度无关。在非零噪声场景中，覆盖概率可以在大尺度衰减参数为 4 时表达成闭式公式，并且这个公式使用了 Q(x)函数，即标准正态分布的结尾概率函数。数值结果表明，全双工通信技术的网络容量增益随着节点密度增加而减少。这一点与无线自组织网络相同。此外，随着链路信噪比增加，全双工通信技术的网络容量增益减少。但在基站天线上使用互干扰消除技术后，全双工通信技术的网络容量增益明显增加。因此，来自全双工通信的网络容量增益是非常有限的，而且互干扰消除技术可以明显提高网络容量增益。

Contents

List of Figures

Chapter 1

Introduction

With the rapid development of wireless communication technologies, wireless networks (e.g., WiFi, and cellular systems) have been widely deployed all around our daily life. Increasing demands for high speed data applications (e.g., online chatting) and growing numbers of users require wireless networks to support high data rate services effectively and efficiently. To achieve this goal, researchers have studied the feasibility of full duplex communications by combatting self-interference in [Everett et al. (2011); Choi et al. (2010); Jain et al. (2011); Bharadia et al. (2013)]. While most works strive to design high performance full duplex radios, we focus on analyzing network layer capacity gain of full duplex communications in large scale wireless networks in the thesis.

The following three sections will firstly introduce a brief history of full duplex wireless communication technique while presenting challenges to study network layer capacity gain of full duplex communication in large scale wireless networks, then show three network capacity analysis approaches and explain the key reason to adopt the approach of stochastic geometry, and give the organization of the thesis at last.

1.1   Brief History of Full Duplex Wireless Communication

During the past two decades, full duplex wireless communication is one of the most emerging techniques in the area of wireless communication and networking. The first full duplex communication system is implemented as full duplex relay by exploiting antenna directionality in [Everett et al. (2011)], but it is limited to directional communications. To achieve omini-directional full duplex communication, self-interference needs to be canceled on the radio, which essentially is to subtract known self-interference signal from the target received signal.

The first practical full-duplex wireless system [Choi et al. (2010)] was realized through the combination of antenna cancelation, radio frequency (RF) cancelation, and digital cancelation technologies. Three antennas, including one receiving and two transmitting antennas, are employed for antenna cancelation. The locations of antennas need to be placed carefully, so that the same transmitting signals from two antennas superpose destructively at the receiving antenna. The noise cancelation chip (Qhx220) [Radunovic et al. (2010)], an interference cancelation circuit, is used to remove the known analog interfered signal from the received signals, and RF cancelation is performed before digital cancelation so that no saturation happens at the digital-to-analogue converter (ADC). Digital cancelation technique, that subtracts known transmitted samples from received digital samples, have been widely studied in literatures, such as ZigZag [Gollakota and Katabi (2008)]. Due to precise location requirement of antennas for cancelation, this primary prototype for full duplex communication is restricted within a small bandwidth. To solve these problems, a new full duplex radio is designed in [Jain et al. (2011)] by introducing signal inversion technique through the balun circuits, i.e. balun cancelation. Thus, the design in [Jain et al. (2011)] can achieve full duplex communication with wider bandwidth. The most advanced design and implementation of full duplex radio is the first in-band full duplex WiFi radio [Bharadia et al. (2013)], which can simultaneously transmit and receive on the same channel using standard WiFi 802.11ac PHYs.

Theoretically, full duplex communication doubles the link throughput due to the feasibility
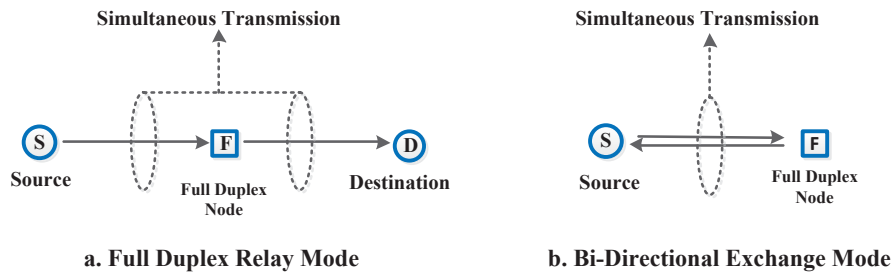
Figure 1.1: Two modes of full duplex communications.

of simultaneous transmission and reception on the same frequency. Practical implementation verifies this expectation and shows 84% improvement of link throughput in [Choi et al. (2010)]. However, it is still an open research topic to identify the network capacity gain of full duplex communication in large scale wireless networks. In [Ju et al. (2012)], end-to-end delay and throughput are analyzed for a multi-hop network. But the analytical model is based on the assumption that any interfering pair of nodes are located at the same position asymptotically as the network density approaching zero in the full duplex network. Thus, it cannot reveal the network capacity for a given network density.

The key challenge to study network capacity gain of full duplex communication is the complicated aggregate network interference. Compared with half duplex communication, more opportunities are created for possible transmissions and receptions in full duplex wireless networks. Moreover, for any wireless terminal with a full duplex radio, two communication modes [Ju et al. (2012)] can be chosen for full duplex communications, i.e., full duplex relay (FDR) mode and bi-directional exchange (BDE) mode (see Fig. 1.1), thus, making the research topic more challenging.

1.2   Capacity Analysis of Wireless Networks via Stochastic Geometry

The most popular approach to model specific physical layer techniques' effects on wireless network capacity is the scaling law framework, which is firstly proposed by Prof. P. R. Kumar in [Gupta and Kumar (2000)]. The network capacity is measured by transport capacity, defined by the sum of products of information bits and transmission distances in unit area. The network topology is modeled as n identical randomly located nodes on a specific two dimensional disk, or a three dimensional sphere with unit area. The analytical results are derived in scaling law forms, which state that transport capacity of wireless network scales with n follows some rule of $\Theta(f(n))$, where $f(n)$ is a polynomial of n. In other word, no exact results can be computed by this framework. Thus, limited design insight can be gained. If we utilize the scaling law framework, it is impossible to identify the specific network capacity gain of full duplex communication over half duplex communications, which supposedly lies in the range $[1, 2]$.

Another approach is the network analysis with fixed geometry, such as the Wyner model for cellular networks [Wyner (1994)], where one-dimensional linear cellular array and two-dimensional hexagonal grid array are used to model the network topology. Concrete capacity results are derived. However, the generality is lost, because the proposed framework can not be applied to another wireless network if the network topology doesn't fit fixed geometry model. Moreover, it is impossible to enumerate all network geometry models.

The approach we adopt in this thesis is via stochastic geometry [Martin et al. (2009)], where network topology is modeled as a random point process and derive the network capacity via theory of stochastic geometry [Stoyan et al. (1995); Martin (2012)]. It has two-fold advantages over the two approaches, scaling law approach and network analysis with fixed geometry approach. Firstly, random point process generalizes the network topology assumption and eliminates the

effects of network topology on network capacity. Secondly, since accurate model for physical layer setting and medium access control protocol are described via stochastic geometry theory, insights for network design are easy to obtain from closed-from analytical results.

Varieties of random point processes are used to model network topology [Martin and Ganti (2009)]. The most popular point process is homogeneous Poisson point process with intensity λ on the plane, which describes an independent and uniform deployment of wireless terminals for the basic topology of wireless network. To achieve the spatial distribution of active concurrent transmissions, the theory of operations on point process is adopted to model the function of medium access control protocols (MAC). Widely adopted MAC protocol is slotted ALOHA [Abramson (1970)], which is simple and effective. When a terminal has a packet to send, it decides to transmit with access probability p independently. Independent thinning theory from stochastic geometry is applied for the wireless networks using ALOHA protocol, and a new Poisson point process is used to model the concurrent transmitters [Baccelli and Blaszczyszyn (2009)]. Widely used CSMA/CA protocol [Colvin (1983)] is modeled by introducing the Hard-core point process based on Poisson process [Nguyen et al. (2007)].

To calculate network capacity, the aggregate interference on a typical link from all the other concurrent transmissions needs to model. Under the framework of stochastic geometry, Palm theory [Stoyan et al. (1995)], i.e. conditional probability of point process, can help to identify the aggregate interference through the spatial distribution of interfering terminals from the view of the typical receiver. As for the interference from a specific terminal, all physical layer settings need to consider, including transmitting power, and wireless channel fading. The wireless channel fading is modeled into two types of fading, the large scale fading and the small scale fading [Tse and Viswanath (2005)]. Rayleigh fading with unit mean is assumed for the small scale fading, while large scale fading is represented by a path loss function $g(r)$ respecting to link distance r. Then, the closed-form aggregate interference is presented and proved to following a shot-noise process [Lowen and Teich (1990)]. Campbell theory [Campbell

(1909)] provides theoretical basis to investigate properties of the aggregate interference, such as the mean and variance.

Different from network capacity model via stochastic geometry for half duplex wireless networks, no aggregate interference model exits for full duplex wireless networks, which is the research task we will work on to identify network capacity gain of full duplex communication. In this thesis, two new aggregate interference models are put forward to fit for two types of full duplex wireless networks, ad hoc network with BDE mode and cellular network with FDR mode, respectively.

1.3   Organization of the Thesis

The rest of this thesis is organized as follows.

In Chapter 2, network capacity of a full duplex wireless ad hoc network, measured by transmission capacity, is investigated. The tail probability of the aggregate interference is presented, and it is indicated that severe network interference is more likely happened in full duplex communication networks. Comparison between half duplex and full duplex transmission capacity is conducted, and analytical and numerical results indicate the limited network capacity gain of full duplex communication in the large scale ad hoc network.

In Chapter 3, network capacity of a full duplex wireless cellular network, measured by average rate of a typical link, is investigated. Mutual interference cancelation technique is put forward between the base stations to relieve severe aggregate interference. Based on proposed model, average rate and coverage probability of a typical uplink and downlink in half duplex and full duplex communication scenarios are derived and compared. Analytical and numerical results indicate the limited network gain of full duplex communication, and the effective improvement of mutual interference cancelation technique on network capacity in the large scale cellular network.

The thesis is concluded in Chapter 4.

Chapter 2

Transmission Capacity of Full Duplex Wireless Ad Hoc Networks

In this chapter, transmission capacity of full duplex wireless ad hoc networks via stochastic geometry is presented. Taking BDE mode of full duplex communications into consideration, Thomas cluster point process is set as network topology and simplified slotted ALOHA is the medium access control protocol. Inter-cluster aggregate interference on the typical link can no longer be modeled by Palm theory, but redefined cluster palm theory. moreover, traditional transmission capacity is generalized into double cases: original maximum transmission throughput by maximizing concurrent transmission density for fixed transmission rate and maximum transmission throughput by maximizing transmission rate for fixed network density. For both definitions of transmission capacity, design aspects of full duplex communication and half communication are compared and analyzed in the wireless ad hoc network.

2.1 Motivation

Wireless ad hoc network is a network formed without any centralized control and self-organized to communicate with each other. Each wireless terminal participates in routing by forwarding

data to other nodes dynamically based on the connectivity of the networks. Emerging full duplex communication techniques bring another degree of freedom on data transmission schemes, since there are two full duplex communication modes, BDE mode and FDR mode, to choose for any node with full duplex radio. Thus, compared with half duplex communication, network capacity of full duplex communication is more challenging to explore.

The vital factor on analyzing network capacity gain is complicated aggregate interference in wireless ad hoc network, since the interference affects link decoding process, which follows the Shannon capacity rule [Shannon (2001)]. Thus, to study the network capacity gain of full duplex wireless ad hoc networks, we first need to fix the model for the complex aggregate interference, then to identify properties of the aggregate interference, such as the statistical distribution function [Win et al. (2009)] and the tail distribution [Ganti and Haenggi (2009)]. However, all existing models for the aggregate interference are conducted for half duplex wireless ad hoc networks and related work on aggregate interference analysis for full duplex wireless networks is lacking. Therefore, modeling aggregate interference in full duplex wireless networks is the primary challenging problem to network capacity gain.

To evaluate network capacity, transmission capacity is widely adopted as the performance metric, which is first introduced for half duplex wireless networks in [Weber et al. (2005)] and defined as the maximum throughput in an unit area, subjecting to a fixed link rate and a constraint of outage probability. Transmission capacity characterizes the maximum spatial transmission throughput that can be supported under certain quality of service (QoS) in wireless networks. However, transmission capacity in full duplex wireless network is still not defined. Thus, how to characterize transmission capacity in full duplex wireless networks is the second challenging problem for us to get the network capacity gain.

Most of existing work on network throughput in full duplex wireless networks are based specific network topologies within small scale, such as Contraflow [Radunovic et al. (2009)] and FD-MAC [Kim and Stark (2013)]. In [Ju et al. (2012)], end-to-end delay and throughput

are analyzed for a large scale multi-hop network. However, the analytical model is based on the assumption that an interfering pair of nodes in full duplex networks are located at the same position asymptotically as network density approaching zero. Thus, it cannot reveal the network throughput gain for large scale full duplex wireless networks. To the best of our knowledge, the impact of full duplex communications on network capacity gain has not been researched for large scale full duplex wireless networks. To study this problem, we need to

- Find an appropriate spatial point process to characterize the network topology for the large scale full duplex wireless ad hoc networks;

- Construct modified Palm theory to construct the shot-noise process for aggregate interference in large scale full duplex wireless ad hoc networks;

- Derive the transmission capacity for both half duplex and full duplex communications.

The main contributions of this section are summarized as follows. We leverage the Thomas cluster point process to model the wireless terminals in full duplex wireless networks. Based on the Thomas cluster point process, a new aggregate interference model is developed and the property of the aggregate interference's tail distribution is explored. The transmission capacity is derived based on this interference model. Comparisons between transmission capacity half duplex and full duplex networks are conducted numerically, which reveal the limitations of full duplex communications in large scale wireless ad hoc networks.

The rest of this chapter is organized as follows. System models are described in Section 2.2. The new aggregate interference model and the asymptotic property of interference's tail distribution are derived in Section 2.3. Based on the aggregate interference model, the successful transmission probability of the typical link is presented in Section 2.4. The equivalence for transmission capacity analysis between Poisson cluster point process and Poisson point process under half duplex communications is illustrated in Section 2.5. Transmission throughput and transmission capacity are derived in Section 2.6. Numerical results are presented in Section

2.7, where limitations of full duplex communications are revealed. The chapter is summarized in Section 2.8.

2.2   System Model

The system model is described in four aspects, including the network topology, the physical layer setting, the distance of typical link, and medium access control protocols.

2.2.1   Network Topology

For half duplex communications, the network topology model is usually Poisson point process, which assumes that the transmitters are distributed in the space uniformly [Martin et al. (2009)]. Considering a full duplex wireless network with BDE mode, every two terminals are paired within a communication distance to achieve full duplex communications. This feature leads to a network topology with clustering property. Thus, Thomas cluster point process [Stoyan et al. (1995)] is adopted as the network topology model on a two-dimensional plane. It is constructed by homogeneous independent clustering, which are applied to a parent point process. The parent point process $\Phi_p = \{\mathbf{x}_1, \mathbf{x}_2, ...\}$ is stationary Poisson process with intensity λ_p, as showed by five-pointed stars in Fig. 2.1. The clusters are of the form $C^{\mathbf{x}_i} = C_i + \mathbf{x}_i = \{\mathbf{x} + \mathbf{x}_i : \mathbf{x} \in C_i\}$ for each $\mathbf{x}_i \in \Phi_p$. The $\{C_i\}$ are a family of identical and independently distributed finite point sets. In this paper, there are two points in each C_i, which are scattered independently and identically following normal distribution $f(\mathbf{x})$ around the origin. The normal distribution $f(\mathbf{x})$ is given by

$$f(\mathbf{x}) = \frac{1}{2\pi\sigma^2} \exp\left(-\frac{\|\mathbf{x}\|^2}{2\sigma^2}\right). \tag{2.1}$$

with mean $(0,0)$, and variance matrix $\begin{pmatrix} \sigma^2 & 0 \\ 0 & \sigma^2 \end{pmatrix}$. Thus, there are two daughter points scattered around its parent point with normal distribution in each cluster, depicted as green circles in
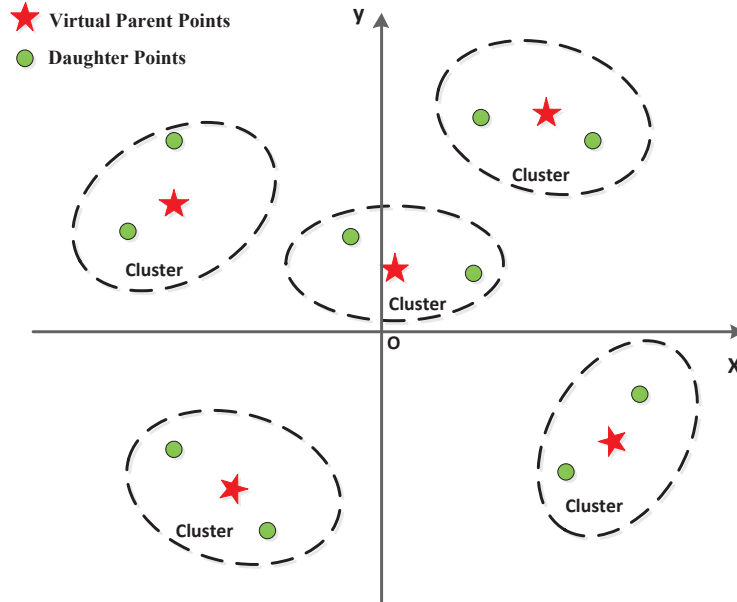
Figure 2.1: Thomas cluster point process with two daughter points in each cluster.

Fig. 2.1. Note that Thomas cluster process only includes daughter points and parent points are just virtual marks. Hence, Thomas cluster point process is given by

$$\Phi = \bigcup_{\mathbf{x}_i \in \Phi_p} C^{\mathbf{x}_i} \tag{2.2}$$

where $C^{\mathbf{x}_i} = C_i + \mathbf{x}_i = \{\mathbf{x} + \mathbf{x}_i : \mathbf{x} \in C_i\}$ and $\mathbf{x}$ follows normal distribution $f(\mathbf{x})$.

2.2.2   Physical Layer Setting

Assume all terminals transmit with the same power P, and the transmission bandwidth is B, while the background noise W is Gaussian with power spectrum density $\frac{N_0}{B}$. Hence, the received noise power is N_0. To model signal propagation through the wireless channel, two types of fading are considered: small-scale fading and large-scale fading. Rayleigh channel fading with unit mean captures small scale fading, while large-scale fading is represented by a

path attenuation model. If a transmitter X at location $\mathbf{x}$ tries to send symbols to a receiver Y at location $\mathbf{y}$, the received power at Y is $P \cdot h_{XY} \cdot g(\mathbf{y} - \mathbf{x})$, where h_{XY} is the power fading coefficient associated with the wireless channel between terminal X and Y, and $g(\mathbf{x}) : \mathbb{R}^2 \to \mathbb{R}^+$ is the path-loss function, representing the path attenuation model and satisfying following the conditions [Ganti and Haenggi (2009)]:

1. $g(\mathbf{x})$ is a continuous, positive, non-increasing function of $\|\mathbf{x}\|$ and

$$\int_{\mathbb{R}^2 \backslash B(o, \epsilon)} g(\mathbf{x}) d\mathbf{x} < \infty, \forall \epsilon > 0$$

   where $B(o, \epsilon)$ is a ball of radius ϵ around the origin.

2. $\lim\limits_{\|\mathbf{x}\| \to \infty} \frac{g(\mathbf{x})}{g(\mathbf{x}-\mathbf{y})} = 1, \forall \mathbf{y} \in \mathbb{R}^2.$

Commonly used path-loss functions include $\|\mathbf{x}\|^{-\alpha}$, $(1 + \|\mathbf{x}\|^{\alpha})^{-1}$, and $\min\{1, \|\mathbf{x}\|^{-\alpha}\}$, which are all normalized for the practical implementation. It is widely accepted that the wireless communication distance is bigger than one wavelength, and the received power attenuates if the communication distance is larger than one wavelength [Schwinger et al. (1998)]. Hence, the path-loss function is chosen as $g(\mathbf{x}) = \frac{a^{\alpha}}{\|\mathbf{x}\|^{\alpha}}$ in the two dimensional network with $\alpha > 2$ and $\|\mathbf{x}\| \geq a$, where a is the wavelength of the electromagnetic wave.

2.2.3   Distance of Typical Link

To derive transmission capacity of wireless networks, we need to focus on the transmission of one link in the wireless network, which is called the typical link. The transmission of the typical link is determined by the aggregate interference from concurrent transmission, Rayleigh channel fading for small scale fading and path attenuation model for large scale fading. The link distance is one of the key factors that determine the path attenuation model. Hence, the link distance affects the transmission of the typical link.

In the network topology of Thomas cluster point process, link distance d_l is the distance between the two points in the cluster. It is known that both two points at locations $\mathbf{x}_1$ and $\mathbf{x}_2$ are distributed identically with two dimensional normal distribution $f(\mathbf{x})$ of zero mean and variance $\begin{pmatrix} \sigma^2 & 0 \\ 0 & \sigma^2 \end{pmatrix}$ around the virtual parent node $\mathbf{z}_0$, i.e., $(\mathbf{x}_2 - \mathbf{z}_0)$ and $(\mathbf{z}_0 - \mathbf{x}_1)$ are two dimensional Gaussian random vectors. Hence, vector $(\mathbf{x}_2 - \mathbf{x}_1)$ is also a Gaussian random vector with mean $(0,0)$ and variance matrix $\begin{pmatrix} 2\sigma^2 & 0 \\ 0 & 2\sigma^2 \end{pmatrix}$. Thus, the link distance $d_l = \|\mathbf{x}_2 - \mathbf{x}_1\|$ is Rayleigh random variable with parameter $\sqrt{2}\sigma$:

$$f_{d_l}(t) = \frac{t}{2\sigma^2} e^{-\frac{t}{4\sigma^2}}. \tag{2.3}$$

2.2.4 Medium Access Control

Slotted ALOHA is considered as the medium access control protocol. To evaluate transmission capacity, it is assumed that every terminal always has packets for its paired target receiver. Link transmissions are active with medium access probability p independently.

In Full duplex communications, the two terminals in one cluster can communicate with each other simultaneously in the same frequency. To make full use of full duplex communications, paired terminals are assumed to start transmission simultaneously. In any time slot, all the potential transmitters forms Thomas cluster point process with two daughters in each cluster. Thus, the networks density is $2\lambda_p$, where λ_p is the density of Parent point process for Thomas cluster point process.

To compare full duplex transmission capacity with half duplex transmission capacity, a slotted ALOHA protocols is designed for half duplex communications under the same network topology of Thomas cluster point process. If the wireless terminal's radio is half duplex, at most one transmission between two paired terminals is permitted in the cluster. Hence, TDD

scheme is used to guarantee both directions of transmission in the cluster. The paired terminals in the cluster take turns to access the spectrum in one time slot. Thus, in any time slot, the potential transmitters form Thomas cluster process with one terminal in each cluster and the network density is λ_p for half duplex communications.

2.3   Aggregate Interference Model

The active transmitters form a new point process after the execution of slotted ALOHA protocols in full duplex communications, which is called independent thinning of the original point process. In the case of Poisson point process model for half duplex communication with density λ, according to independent thinning theorem [Stoyan et al. (1995)], independent thinning with medium access probability p results in a new Poisson point process with density $p\lambda$ for the active transmitters. For the full duplex communications, due to the assumption of correlation between daughter points in the cluster, the independent thinning of Thomas cluster point process can be represented by the independent thinning of virtual Poisson parent point process. The new active virtual parent point process is Poisson point process with density $p\lambda_p$. Thus, the independent thinning of Thomas cluster point process also results in Thomas cluster point process with density of $2p\lambda_p$ in full duplex communications.

To derive full duplex transmission capacity, interference on the typical link from concurrent transmission needs to be investigated. In order to determine the interference, the distribution of all transmissions from the view of the typical link, i.e. palm distribution [Stoyan et al. (1995)], needs to be derived. In the half duplex communications with Poisson point process, Slivnyak's theorem [Stoyan et al. (1995)] provides theoretical basis for the palm distribution. It states that palm distribution of Poisson point process is also Poisson point process with the same density. Thus, all the transmitters that generate interference to the typical link also follow the Poisson point process in half duplex communications.

In the full duplex communications, all wireless terminals are transmitter and receiver at the same time in the network topology of Thomas cluster point process. Therefore, the typical link's receiver is also transmitter in the full duplex network, making the aggregate interference on the typical link to be inter-cluster interference. Traditional Slivnyak's theorem cannot help to derive this inter-cluster aggregate interference. In this section, this problem is solved via the unique construction of Thomas cluster process and Slivnyak's theorem. Based on this new model for the full duplex inter-cluster aggregate interference and the traditional model for half duplex aggregate interference, the asymptotic tail probabilities are derived and comparison of aggregate interference's distribution between full and half duplex communications is conducted at the end of this section.

2.3.1   Inter-cluster Interference in Full Duplex Communications

With slotted ALOHA protocol, active transmitters form Thomas cluster Point process Φ' with density $2p\lambda_p$. Since Thomas cluster point process is stationary, the transmitter of the typical link can be assumed to be located at the origin $\mathbf{o}$ of the plane. We denote the typical cluster as ϕ_o, which contains the typical link, the location of virtual parent point in typical cluster ϕ_o as $\mathbf{z}_p$, and location of the paired receiver as $\mathbf{z}$. Thus, typical link distance is $d = \|\mathbf{z}\|$. Aggregate interference $I(\mathbf{z})$ on the typical receiver is inter-cluster interference, given by

$$I(\mathbf{z}) = \sum_{\mathbf{x}\in\Phi'/\{\phi_o\}} P \cdot h_X \cdot g(\mathbf{x} - \mathbf{z}),$$

where P is the transmitting power, h_X is the power fading coefficient associated with the wireless channel between terminal X and Z, and $g(\mathbf{x})$ is the path-loss function, representing the path attenuation model.

Note that the virtual parent process of Thomas cluster process is Poisson point process. According to Slivnyak's theorem, from the view of typical parent point $\mathbf{z}_p$, all the other parent

points form Poisson point process with density $p\lambda_p$. Thus, from the viewpoint of $\mathbf{z}_p$, the daughter points from all the other clusters form Thomas cluster point process with density $2p\lambda_p$. Since Thomas cluster process is stationary, linear transformation of space cannot change the distribution of point process. Therefore, from the view of typical receiver $\mathbf{z}$, the daughter points from all the other clusters also form Thomas cluster process with the density $2p\lambda_p$. Thus, The aggregate interference on the typical link is equal to interference from all the points in Thomas cluster process. Therefore,

$$I(\mathbf{z}) = \sum_{\mathbf{x} \in \Phi'} P \cdot h_X \cdot g(\mathbf{x} - \mathbf{z}) = \sum_{\mathbf{x} \in \Phi'} P \cdot h_X \cdot g(\mathbf{x}), \tag{2.4}$$

The last equation in E.q. (2.4) results from the fact Thomas cluster point process is stationary.

Based on inter-cluster interference model, the mean and variance of inter-cluster aggregate interference on the typical link are derived in full duplex wireless ad hoc networks.

Theorem 2.1. *Let $\Phi \subset \mathbb{R}^2$ be a Thomas cluster Point Process with two daughters in each cluster. Assuming the parent process density is λ_p, the mean and variance of inter-cluster aggregate interference on typical link for full duplex communications are as follows:*

$$\begin{cases} \mathbb{E}[I(\boldsymbol{z})] = 2p\lambda_p P \int_{\mathbb{R}^2} g(\boldsymbol{x})d\boldsymbol{x}. \\ var[I(\boldsymbol{z})] = 5p\lambda_p P \int_{\mathbb{R}^2} g^2(\boldsymbol{x})d\boldsymbol{x}. \end{cases} \tag{2.5}$$

Proof. First, the mean of inter-cluster aggregate interference is derived.

$$\begin{aligned} \mathbb{E}[I(\mathbf{z})] &= \mathbb{E}\left[\sum_{\mathbf{x} \in \Phi} P h_{\mathbf{x}} g(\mathbf{x} - \mathbf{z}) \right] \\ &= P\mathbb{E}\left[\sum_{\mathbf{y} \in \Phi_p} \left(\sum_{\mathbf{x} - \mathbf{y} \in N_0} g(\mathbf{x} - \mathbf{z}) \right) \right] \\ &= 2\lambda_p P \int_{\mathbb{R}^2} \int_{\mathbb{R}^2} g(\mathbf{x} + \mathbf{y} - \mathbf{z}) f(\mathbf{y}) d\mathbf{y} d\mathbf{x} \\ &= 2\lambda_p P \int_{\mathbb{R}^2} g(\mathbf{x} - \mathbf{z}) d\mathbf{x}. \end{aligned} \tag{2.6}$$

As for variance of inter-cluster aggregate interference, $var[I(\mathbf{z})] = \mathbb{E}[I^2(\mathbf{z})] - \mathbb{E}^2[I(\mathbf{z})]$. We need to calculate $\mathbb{E}[I^2(\mathbf{z})]$.

$$
\begin{aligned}
\mathbb{E}[I^2(\mathbf{z})] &= \mathbb{E}\left[\left(\sum_{\mathbf{x}\in\Phi} Ph_{\mathbf{x}}g(\mathbf{x}-\mathbf{z})\right)\left(\sum_{\mathbf{y}\in\Phi} Ph_{\mathbf{y}}g(\mathbf{y}-\mathbf{z})\right)\right] \\
&= P^2\mathbb{E}\left[\sum_{\mathbf{x}\in\Phi}(h_{\mathbf{x}}g(\mathbf{x}-\mathbf{z}))^2\right] + P^2\mathbb{E}\left[\sum_{\mathbf{x},\mathbf{y}\in\Phi}^{\neq} h_{\mathbf{x}}h_{\mathbf{y}}g(\mathbf{x}-\mathbf{z})g(\mathbf{y}-\mathbf{z})\right]
\end{aligned}
\tag{2.7}
$$

The first term in E.q.(2.7) is calculated as follows

$$
\begin{aligned}
P^2\mathbb{E}\left[\sum_{\mathbf{x}\in\Phi}(h_{\mathbf{x}}g(\mathbf{x}-\mathbf{z}))^2\right] &= \mathbb{E}[h^2]\mathbb{E}\left[\sum_{\mathbf{x}\in\Phi}g^2(\mathbf{x}-\mathbf{z})\right] \\
&= 4\lambda_p P^2 \int_{\mathbb{R}^2}\int_{\mathbb{R}^2} g^2(\mathbf{x}+\mathbf{y}-\mathbf{z})f(\mathbf{y})d\mathbf{x}d\mathbf{y} \\
&= 4\lambda_p P^2 \int_{\mathbb{R}^2} g^2(\mathbf{x}-\mathbf{z})d\mathbf{x}.
\end{aligned}
\tag{2.8}
$$

The second term in E.q.(2.7) is decomposed into two sub-terms A and B by whether $\mathbf{x}$ and $\mathbf{y}$ lie in the same cluster N_0^s:

$$
\mathbb{E}\left[\sum_{\mathbf{x},\mathbf{y}\in\Phi}^{\neq} h_{\mathbf{x}}h_{\mathbf{y}}g(\mathbf{x}-\mathbf{z})g(\mathbf{y}-\mathbf{z})\right] = A + B.
\tag{2.9}
$$

Sub-term A contains the situations when $\mathbf{x}$ and $\mathbf{y}$ lie in the same cluster N_0^s:

$$
\begin{aligned}
A &= \mathbb{E}\left[\sum_{\mathbf{x},\mathbf{y}\in N_0^s\subset\Phi}^{\neq} h_{\mathbf{x}}h_{\mathbf{y}}g(\mathbf{x}-\mathbf{z})g(\mathbf{y}-\mathbf{z})\right] \\
&= \mathbb{E}\left[\sum_{s\in\Phi_p} h_{\mathbf{x}}h_{\mathbf{y}}g(\mathbf{x}-\mathbf{z})g(\mathbf{y}-\mathbf{z})\right] \\
&= \lambda_p \int_{\mathbb{R}^2} g^2(\mathbf{x}-\mathbf{z})d\mathbf{x},
\end{aligned}
\tag{2.10}
$$

Sub-term B contains the situations when $\mathbf{x}$ and $\mathbf{y}$ lie in the different clusters N_0^s:

$$
\begin{aligned}
B &= \mathbb{E}\left[\sum_{\mathbf{x}\in N_0^s\subset\Phi, \mathbf{y}\in N_0^t\subset\Phi}^{s\neq t} h_{\mathbf{x}}h_{\mathbf{y}}g(\mathbf{x}-\mathbf{z})g(\mathbf{y}-\mathbf{z})\right] \\
&= 4\mathbb{E}\left[\sum_{\mathbf{s},\mathbf{t}\in\Phi_p}^{\neq} g(\mathbf{s}-\mathbf{z})g(\mathbf{t}-\mathbf{z})\right] \\
&= 4\left[\lambda_p\int_{\mathbb{R}^2}g(\mathbf{x}-\mathbf{z})d\mathbf{x}\right]^2.
\end{aligned}
\tag{2.11}
$$

Thus,

$$
var[I(\mathbf{z})] = \mathbb{E}[I^2(\mathbf{z})] - \mathbb{E}^2[I(\mathbf{z})] = 5P^2\lambda_p\int_{\mathbb{R}^2}g^2(\mathbf{x}-\mathbf{z})d\mathbf{x}.
\tag{2.12}
$$

$\square$

For half duplex communications, mean and variance of the interference on the typical link are derived in [Martin (2012)]. Comparing those two results, we find that: 1) Mean interference on the typical link in full duplex communications is twice as much as that in half duplex communications with Poisson point process with density λ_p; 2) If half duplex communication network density doubles, i.e. Poisson network density is $2\lambda_p$, the interference on the typical link in half duplex communications and full duplex communications are equal, but the variance of interference on the typical link in full duplex communications is 2.5 times as much as that in half duplex communications.

Thus, compared with half duplex communications, full duplex communications allow more transmission opportunities, but double the mean interference on the typical link and much larger variance.

2.3.2   Aggregate Interference's Tail Probability

To compare the distribution of aggregate interference in half and full duplex wireless networks, the tail probability (CCDF) of aggregate interference $I(\mathbf{z})$, represented by $\bar{F}_I(y) = \mathbb{P}(I(\mathbf{z}) \geq y)$, is planned to explored in this subsection. As transmission power P is constant, it is set to be

unit value to make the analysis simple to derive, i.e. $P = 1$. Firstly, a general theorem is derived for the bounds of interference tail probability when all interferers follow a general spatial point process. Then, the general spatial point process is restricted to Poisson point process for half duplex communications, or Thomas cluster point process for full duplex communications. Comparison on asymptotic order of the aggregate interference's tail probability is conducted between half duplex communications and full duplex communications, which leads to the dispersal of interference in the full duplex wireless network.

Based on the derivation in [Ganti and Haenggi (2009); Sousa and Silvester (1990)], a general results for the bounds of interference's tail probability is presented.

Theorem 2.2. *Let $\Phi' \subset \mathbb{R}^2$ be a stationary spatial point process. Assume that all the points in the process contribute to the interference on a typical link, represented by $I(\boldsymbol{z})$. The tail probability $F_I(y)$ of $I(\boldsymbol{z})$ is lower bounded by $\bar{F}_I^l(y)$ and upper bounded by $\bar{F}_I^u(y)$:*

$$\begin{cases} \bar{F}_I^l(y) = 1 - \mathcal{G}\left(F_h\left(\frac{y}{g(\cdot)}\right)\right) \\ \bar{F}_I^u(y) = 1 - (1 - \varphi(y))\mathcal{G}\left(F_h\left(\frac{y}{g(\cdot)}\right)\right), \end{cases} \tag{2.13}$$

where $F_h(x)$ denotes the CDF of the power fading coefficient h, $\mathcal{G}(f(\cdot))$ is the generating functional of $f(x)$, defined by $\mathcal{G}(f(\cdot)) = \mathbb{E}_{\Phi'}\left[\prod_{\boldsymbol{x} \in \Phi'} f(\boldsymbol{x})\right]$ and

$$\varphi(y) = \frac{1}{y}\mathbb{E}\sum_{\boldsymbol{x} \in \Phi'} g(\boldsymbol{x}) \int\limits_0^{y/g(\boldsymbol{x})} v \, dF_h(v). \tag{2.14}$$

Proof. To obtain the lower and upper bounds of tail probability $F_I(y)$ of $I(\mathbf{z})$, the interferers are divided into two sets, one set ϕ_y with the interferers, whose individual interference is larger than y and the other set ϕ_y^c with the interferers whose individual interference is no more than y, i.e.

$$\phi_y = \{\mathbf{x} \in \Phi', h_x g(\mathbf{x}) > y\}. \tag{2.15}$$

$$\phi_y^c = \{\mathbf{x} \in \Phi', h_x g(\mathbf{x}) \leq y\}. \tag{2.16}$$

Thus, $I(\mathbf{z}) = I_{\phi_y}(\mathbf{z}) + I_{\phi_y^c}(\mathbf{z})$, where $I_{\phi_y}(\mathbf{z})$ corresponds to the interference due to the set ϕ_y and $I_{\phi_y^c}(\mathbf{z})$ corresponds to the interference due to the set ϕ_y^c. Then, by the definition of tail probability, we can get

$$
\begin{aligned}
\bar{F}_I(y) &= \mathbb{P}(I_{\phi_y}(\mathbf{z}) + I_{\phi_y^c}(\mathbf{z}) \geq y) \\
&\geq \mathbb{P}(I_{\phi_y}(\mathbf{z}) \geq y) \\
&= 1 - \mathbb{P}(I_{\phi_y}(\mathbf{z}) < y) \\
&= 1 - \mathbb{P}(\phi_y = \emptyset).
\end{aligned}
\tag{2.17}
$$

Based the results of (2.17), we need to calculate the probability $\mathbb{P}(\phi_y = \emptyset)$. This probability can be transformed into a Laplace functional of the point process:

$$
\begin{aligned}
\mathbb{P}(\phi_y = \emptyset) &= \mathbb{E}\left[\prod_{\mathbf{x} \in \Phi'} 1_{h_\mathbf{x} g(\mathbf{x}) \leq y}\right] \\
&= \mathbb{E}\left[\prod_{\mathbf{x} \in \Phi'} \mathbb{E}_{h_\mathbf{x}}\left(1_{h_\mathbf{x} g(\mathbf{x}) \leq y}\right)\right] \\
&= \mathbb{E}\left[\prod_{\mathbf{x} \in \Phi'} F_h\left(\frac{y}{g(\mathbf{x})}\right)\right] \\
&= \mathcal{G}\left(F_h\left(\frac{y}{g(\cdot)}\right)\right).
\end{aligned}
\tag{2.18}
$$

So the lower bound for the tail probability $\bar{F}_I(y)$ is

$$\bar{F}_I^l(y) = 1 - \mathcal{G}\left(F_h\left(\frac{y}{g(\cdot)}\right)\right). \tag{2.19}$$

Following the derivation for upper bound of tail probability in [Ganti and Haenggi (2009)], we get

$$\bar{F}_I(y) = 1 - (1 - \mathbb{P}(I(\mathbf{z}) > y | I_{\phi_y} \leq y))\mathcal{G}\left(F_h\left(\frac{y}{g(\cdot)}\right)\right) \tag{2.20}$$

and

$$\mathbb{P}(I(\mathbf{z}) > y | I_{\phi_y} \leq y) = \mathbb{P}(I(\mathbf{z}) > y | \phi_y = \emptyset)$$

$$\leq \frac{\mathbb{E}(I(\mathbf{z}) | \phi_y = \emptyset)}{y}$$

$$= \frac{1}{y} \mathbb{E} \sum_{\mathbf{x} \in \Phi'} h_{\mathbf{x}} g(\mathbf{x}) 1_{h_{\mathbf{x}} g(\mathbf{x}) \leq y} \tag{2.21}$$

$$= \frac{1}{y} \mathbb{E} \sum_{\mathbf{x} \in \Phi'} g(\mathbf{x}) \int_0^{y/g(\mathbf{x})} v \, dF_h(v).$$

Hence, we get the upper bound for tail probability $F_I(y)$:

$$\bar{F}_I^u(y) = 1 - (1 - \varphi(y))\mathcal{G}\left(F_h\left(\frac{y}{g(\cdot)}\right)\right), \tag{2.22}$$

where $\varphi(y) = \frac{1}{y} \mathbb{E} \sum_{\mathbf{x} \in \Phi'} g(\mathbf{x}) \int_0^{y/g(\mathbf{x})} v \, dF_h(v).$ $\qquad \square$

In half duplex networks, the wireless terminals are assumed to follow Poisson point process, meaning that they are distributed in the space uniformly. From the view of typical receiver, the interferers form Poisson point process with the same density as the original point process, which follows the Palm theory. If the network density is λ, we can get the lower and upper bounds of tail probability $F_I(y)$ of $I(\mathbf{z})$.

Corollary 2.2.1. *Let the half duplex network topology follows a Poisson point process $\Phi' \subset \mathbb{R}^2$ with density λ. The tail probability $F_I(y)$ of $I(\mathbf{z})$ is lower bounded by $\bar{F}_I^{lH}(y)$ and upper bounded by $\bar{F}_I^{uH}(y)$:*

$$\begin{cases} \bar{F}_I^{lH}(y) = 1 - \mathcal{G}^H\left(F_h\left(\frac{y}{g(\cdot)}\right)\right) \\ \bar{F}_I^{uH}(y) = 1 - (1 - \varphi^H(y))\mathcal{G}^H\left(F_h\left(\frac{y}{g(\cdot)}\right)\right), \end{cases} \tag{2.23}$$

where $\mathcal{G}^H\left(F_h\left(\frac{y}{g(\cdot)}\right)\right) = \exp\left[-\lambda \int_{\mathbb{R}^2}\left(1 - F_h\left(\frac{y}{g(\boldsymbol{x})}\right)\right) d\boldsymbol{x}\right]$ *and* $\varphi^H(y) = \frac{\lambda}{y} \int_{\mathbb{R}^2} g(\boldsymbol{x}) \int_0^{y/g(\boldsymbol{x})} v \, dF_h(v) d\boldsymbol{x}.$

Proof. The results are based on the generating functional of Poisson point process and the mean sum over the point process [Martin (2012)]. $\qquad \square$

In the similar way, we can get the lower and upper bounds of tail probability $F_I(y)$ of $I(\mathbf{z})$ when the general point process is restricted to Thomas cluster point process for full duplex communications.

Corollary 2.2.2. *Let $\Phi' \subset \mathbb{R}^2$ be a Thomas cluster point process with parent node density λ_p and two daughter nodes in each cluster. The tail probability $F_I(y)$ of $I(\mathbf{z})$ is lower bounded by $F_I^{lF}(y)$ and upper bounded by $F_I^{uF}(y)$:*

$$
\begin{cases}
\bar{F}_I^{lF}(y) = 1 - \mathcal{G}^F \left(F_h \left(\frac{y}{g(\cdot)} \right) \right) \\
\bar{F}_I^{uF}(y) = 1 - (1 - \varphi^F(y)) \mathcal{G}^F \left(F_h \left(\frac{y}{g(\cdot)} \right) \right)
\end{cases}
\tag{2.24}
$$

where $\mathcal{G}^F \left(F_h \left(\frac{y}{g(\cdot)} \right) \right) = \exp \left(-\lambda_p \int_{\mathbb{R}^2} \left[1 - \left(\int_{\mathbb{R}^2} F_h \left(\frac{y}{g(\boldsymbol{x}+\boldsymbol{z})} \right) f(\boldsymbol{z}) d\boldsymbol{z} \right)^2 \right] d\boldsymbol{x} \right)$ *and* $\varphi^F(y) = \frac{2\lambda_p}{y} \int_{\mathbb{R}^2} g(\boldsymbol{x}) \int_0^{y/g(\boldsymbol{x})} v dF_h(v) d\boldsymbol{x}.$

Proof. The results are based on the generating functional of Thomas cluster point process and the mean sum over the point process [Ganti and Haenggi (2009)]. $\qquad\square$

To confirm the tightness of the lower and upper bounds for the tail distribution of interference in both half duplex and full duplex networks, we derive the asymptotic order for the bounds when y approaches infinity. The following theorem shows that aggregate interference in full duplex networks has the same asymptotic order as the aggregate interference in half duplex networks.

Theorem 2.3. *For $g(x) = \frac{a^\alpha}{\|x\|^\alpha}$ with $\alpha \geq 2$ and $\|\boldsymbol{x}\| \geq a$, where a is the wavelength of the electric wave. The lower and upper bounds to CCDF $\bar{F}_I(y)$ of the interference in full duplex and half duplex networks scales as follows for $y \to \infty$:*

$$
\begin{cases}
\bar{F}_I^{lH}(y) \sim \pi \lambda a^2 [F_h(y) - 1] + \pi \lambda a^2 y^{-\frac{2}{\alpha}} C(y) \\
\bar{F}_I^{uH}(y) \sim \pi \lambda a^2 [F_h(y) - 1] + \frac{\alpha}{\alpha-2} \pi \lambda a^2 y^{-\frac{2}{\alpha}} C(y).
\end{cases}
\tag{2.25}
$$

and

$$\begin{cases} \bar{F}_I^{lF}(y) \sim \pi\lambda a^2[F_h(y) - 1] + \pi\lambda a^2 y^{-\frac{2}{\alpha}} C(y) \\ \bar{F}_I^{uF}(y) \sim 2\pi\lambda a^2[F_h(y) - 1] + \frac{2\alpha}{\alpha-2}\pi\lambda a^2 y^{-\frac{2}{\alpha}} C(y). \end{cases} \tag{2.26}$$

where $C(y) = \int_y^\infty t^{\frac{2}{\alpha}} dF_h(t)$.

Proof. For the lower bound $\bar{F}_I^{lH}(y)$, the Laplace function term is expanded as follow:

$$\mathcal{G}^F\left(F_h\left(\frac{y}{g(\cdot)}\right)\right) = \exp\left[-\lambda \int_{\mathbb{R}^2}\left(1 - F_h\left(\frac{y}{g(\mathbf{x})}\right)\right) d\mathbf{x}\right] \tag{2.27}$$

When $y \to \infty$, then $F_h\left(\frac{y}{g(\mathbf{x+z})}\right) \to 1$, making the whole parameter in exponential function to be 0. Due to the fact $\exp(-x) \sim 1 - x$, when $x \to 0$, hence

$$\mathcal{G}^H\left(F_h\left(\frac{y}{g(\cdot)}\right)\right) \sim 1 - M^H(y) = 1 - \lambda \int_{\mathbb{R}^2}\left(1 - F_h\left(\frac{y}{g(\mathbf{x})}\right)\right) d\mathbf{x}. \tag{2.28}$$

Therefore, taking the form of path-loss function $g(\mathbf{x})$ into the lower bound $\bar{F}_I^{lH}(y)$, we can get:

$$\begin{aligned} \bar{F}_I^{lH}(y) &\sim M^H(y) = \lambda \int_{\mathbb{R}^2}\left(1 - F_h\left(\frac{y}{g(\mathbf{x})}\right)\right) d\mathbf{x} \\ &= 2\pi\lambda \int_a^\infty r\left(1 - F_h\left(\frac{yr^\alpha}{a^\alpha}\right)\right) dr \\ &= \pi\lambda a^2 y^{-\frac{2}{\alpha}} \int_y^\infty [1 - F_h(t)] dt^{\frac{2}{\alpha}} \\ &= \pi\lambda a^2[F_h(y) - 1] + \pi\lambda a^2 y^{-\frac{2}{\alpha}} \int_y^\infty t^{\frac{2}{\alpha}} dF_h(t). \end{aligned} \tag{2.29}$$

For the upper bound $\bar{F}_I^{uF}(y)$, let's consider the asymptotic order of $\varphi^H(y)$ when $y \to \infty$:

$$\begin{aligned} \varphi^H(y) &= \frac{\lambda}{y} \int_{\mathbb{R}^2} g(\mathbf{x}) \int_0^{y/g(\mathbf{x})} v dF_h(v) d\mathbf{x} \\ &= \frac{\lambda}{y} \int_{\|\mathbf{x}\| \geq a} \frac{a^\alpha}{\|\mathbf{x}\|^\alpha} \int_0^{\frac{y\|\mathbf{x}\|^\alpha}{a^\alpha}} v dF_h(v) d\mathbf{x} \\ &= \frac{2\pi\lambda}{y} \int_a^\infty \frac{a^\alpha}{r^{\alpha-1}} \int_0^{\frac{yr^\alpha}{a^\alpha}} v dF_h(v) dr \\ &= \frac{2\pi\lambda}{y} \int_y^\infty \int_{a\left(\frac{v}{y}\right)^{\frac{1}{\alpha}}}^\infty \frac{a^\alpha}{r^{\alpha-1}} v dr dF_h(v) \\ &= \frac{2\pi\lambda a^2 y^{-\frac{2}{\alpha}}}{\alpha-2} \int_y^\infty v^{\frac{2}{\alpha}} dF_h(v). \end{aligned} \tag{2.30}$$

Based on the representation of upper bound $\bar{F}_I^{uH}(y)$, we can get

$$
\begin{aligned}
\bar{F}_I^{uH}(y) &= 1 - (1 - \varphi^H(y))\mathcal{G}^H\left(F_h\left(\frac{y}{g(\cdot)}\right)\right) \\
&\sim 1 - (1 - \varphi^H(y))(1 - M^H(y)) \\
&= \varphi^H(y) + M^H(y) - \varphi^H(y) \cdot M^H(y) \\
&\sim \varphi^H(y) + M^H(y) \\
&= \pi\lambda a^2[F_h(y) - 1] + \frac{\alpha\pi\lambda a^2 y^{-\frac{2}{\alpha}}}{\alpha - 2}\int_y^\infty v^{\frac{2}{\alpha}}dF_h(v).
\end{aligned}
\tag{2.31}
$$

For the lower bound $\bar{F}_I^{lF}(y)$, the Laplace function term is expanded as follow:

$$
\mathcal{G}^H\left(F_h\left(\frac{y}{g(\cdot)}\right)\right) \sim 1 - M^F(y) = 1 - \lambda_p\int_{\mathbb{R}^2}\left[1 - \left(\int_{\mathbb{R}^2}F_h\left(\frac{y}{g(\mathbf{x+z})}\right)f(\mathbf{z})d\mathbf{z}\right)^2\right]d\mathbf{x}.
\tag{2.32}
$$

According to the property of cumulative distribution function, $F_h\left(\frac{y}{g(\mathbf{x+z})}\right) \in [0,1]$, then the value of $\int_{\mathbb{R}^2}F_h\left(\frac{y}{g(\mathbf{x+z})}\right)f(\mathbf{z})d\mathbf{z}$ lies in $[0,1]$, $\forall \mathbf{x} \in \mathbb{R}^2$. So

$$
\begin{aligned}
&1 - \left(\int_{\mathbb{R}^2}F_h\left(\frac{y}{g(\mathbf{x+z})}\right)f(\mathbf{z})d\mathbf{z}\right)^2 \\
&= \left[1 + \left(\int_{\mathbb{R}^2}F_h\left(\frac{y}{g(\mathbf{x+z})}\right)f(\mathbf{z})d\mathbf{z}\right)\right] \times \left[1 - \left(\int_{\mathbb{R}^2}F_h\left(\frac{y}{g(\mathbf{x+z})}\right)f(\mathbf{z})d\mathbf{z}\right)\right] \\
&\geq \left[1 - \left(\int_{\mathbb{R}^2}F_h\left(\frac{y}{g(\mathbf{x+z})}\right)f(\mathbf{z})d\mathbf{z}\right)\right].
\end{aligned}
\tag{2.33}
$$

Then

$$
\begin{aligned}
1 - M^F(y) &\leq 1 - \lambda_p\int_{\mathbb{R}^2}\left[1 - \left(\int_{\mathbb{R}^2}F_h\left(\frac{y}{g(\mathbf{x+z})}\right)f(\mathbf{z})d\mathbf{z}\right)\right]d\mathbf{x} \\
&= 1 - \lambda_p\int_{\mathbb{R}^2}\left[1 - F_h\left(\frac{y}{g(\mathbf{x})}\right)\right]d\mathbf{x} \\
&= 1 - M^H(y).
\end{aligned}
\tag{2.34}
$$

Based on the representation of lower bound $\bar{F}_I^{lF}(y)$, we can get

$$
\begin{aligned}
\bar{F}_I^{lF}(y) &= 1 - \mathcal{G}\left(F_h\left(\frac{y}{g(\cdot)}\right)\right) \sim M^F(y) \geq M^H(y) \\
&= \pi\lambda a^2[F_h(y) - 1] + \pi\lambda a^2 y^{-\frac{2}{\alpha}}\int_y^\infty t^{\frac{2}{\alpha}}dF_h(t).
\end{aligned}
\tag{2.35}
$$

For the upper bound $\bar{F}_I^{uF}(y)$, let's consider the asymptotic order of $\varphi^F(y)$ when $y \to \infty$:

$$\varphi^F(y) = \frac{2\lambda_p}{y} \int_{\mathbb{R}^2} g(\mathbf{x}) \int_0^{y/g(\mathbf{x})} v \, dF_h(v) d\mathbf{x} = \frac{4\pi\lambda a^2 y^{-\frac{2}{\alpha}}}{\alpha-2} \int_y^\infty v^{\frac{2}{\alpha}} dF_h(v). \tag{2.36}$$

To get the upper bound $\bar{F}_I^{uF}(y)$, we make use of boundedness of cumulative density function. $\int_{\mathbb{R}^2} F_h\left(\frac{y}{g(\mathbf{x+z})}\right) f(\mathbf{z}) d\mathbf{z}$ lies in $[0,1]$, $\forall x \in \mathbb{R}^2$. So

$$\begin{aligned}
&1 - \left(\int_{\mathbb{R}^2} F_h\left(\frac{y}{g(\mathbf{x+z})}\right) f(\mathbf{z}) d\mathbf{z}\right)^2 \\
&= \left[1 + \left(\int_{\mathbb{R}^2} F_h\left(\frac{y}{g(\mathbf{x+z})}\right) f(\mathbf{z}) d\mathbf{z}\right)\right] \cdot \left[1 - \left(\int_{\mathbb{R}^2} F_h\left(\frac{y}{g(\mathbf{x+z})}\right) f(\mathbf{z}) d\mathbf{z}\right)\right] \\
&\leq 2 \cdot \left[1 - \left(\int_{\mathbb{R}^2} F_h\left(\frac{y}{g(\mathbf{x+z})}\right) f(\mathbf{z}) d\mathbf{z}\right)\right].
\end{aligned} \tag{2.37}$$

Then

$$\begin{aligned}
1 - M^F(y) &\geq 1 - 2\lambda_p \int_{\mathbb{R}^2} \left[1 - \left(\int_{\mathbb{R}^2} F_h\left(\frac{y}{g(\mathbf{x+z})}\right) f(\mathbf{z}) d\mathbf{z}\right)\right] d\mathbf{x} \\
&= 1 - 2\lambda_p \int_{\mathbb{R}^2} \left[1 - F_h\left(\frac{y}{g(\mathbf{x})}\right)\right] d\mathbf{x} \\
&= 1 - 2\pi\lambda_p a^2 y^{-\frac{2}{\alpha}} \left[-y^{\frac{2}{\alpha}}[1 - F_h(y)] + \int_y^\infty t^{\frac{2}{\alpha}} dF_h(t)\right].
\end{aligned} \tag{2.38}$$

Hence,

$$M^F(y) \leq 2\pi\lambda a^2 y^{-\frac{2}{\alpha}} \left[-y^{\frac{2}{\alpha}}[1 - F_h(y)] + \int_y^\infty t^{\frac{2}{\alpha}} dF_h(t)\right]. \tag{2.39}$$

Similar to the derivation for upper bound $\bar{F}_I^{uH}(y)$, we can get

$$\begin{aligned}
\bar{F}_I^{uF}(y) &\sim \varphi^F(y) + M^F(y) \\
&\leq 2\pi\lambda a^2[F_h(y) - 1] + \frac{2\alpha\pi\lambda a^2 y^{-\frac{2}{\alpha}}}{\alpha-2} \int_y^\infty v^{\frac{2}{\alpha}} dF_h(v).
\end{aligned} \tag{2.40}$$

Then, we can loose the upper bound so that

$$\bar{F}_I^{uH}(y) \sim 2\pi\lambda a^2[F_h(y) - 1] + \frac{2\alpha\pi\lambda a^2 y^{-\frac{2}{\alpha}}}{\alpha-2} \int_y^\infty v^{\frac{2}{\alpha}} dF_h(v). \tag{2.41}$$

$\square$
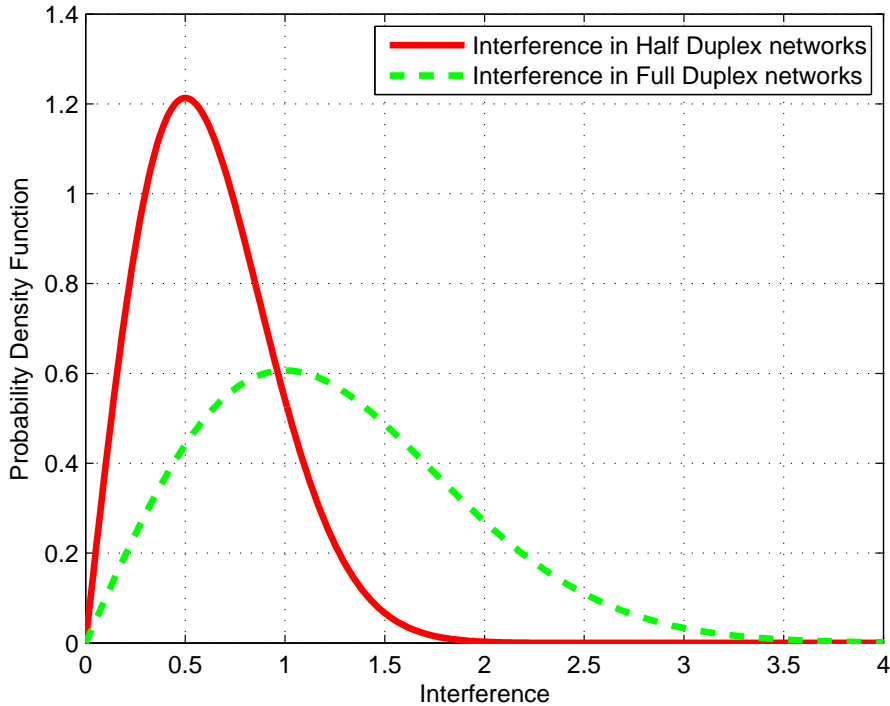
Figure 2.2: Interference Distributions of full duplex and half duplex communications.

Theorem 2.3 implies that the lower bounds of interference's tail probability in full duplex and half duplex networks are equal, and upper bounds of interference's tail probability in full duplex and half duplex networks are in the same order. Moreover, in both half duplex and full duplex communication networks, the upper and lower bounds on interference's tail probability have the same asymptotic order. Therefore, the tail probabilities of interference in half duplex and full duplex networks are approximately the same when interference is large enough.

From the Theorem 2.1, the means and variances of interference full duplex networks are larger than that in half duplex networks. Depicted in Fig. 2.2, when the value of interference are large enough, the tail probabilities of interference in half duplex and full duplex networks are approximately the same. So it can be concluded that full duplex communication makes the distribution of aggregate interference more dispersed when comparing with half duplex communications in wireless ad hoc networks.

2.4 Successful Transmission Probability in Full Duplex Networks

2.4.1 Successful Transmission Probability

As depicted in E.q. (2.4), the aggregate interference on the typical link is equal to interference from all clusters in Thomas cluster point process, i.e.

$$I(\mathbf{z}) = \sum_{\mathbf{x} \in \Phi'} P \cdot h_X \cdot g(\mathbf{x}).$$

Thus, the aggregate interference $I(\mathbf{z})$ follows a shot-noise process [Lowen and Teich (1990)]. Successful transmission occurs if the received signal interference plus noise ratio (SINR) is large than a threshold T, which is decided by a fixed transmission rate requirement. The transmission distance is d. Hence, the probability of successful transmission $\mathbb{P}_{suc}(\mathbf{z})$ is represented by

$$\mathbb{P}_{suc}^{Full}(d, T) = \mathbb{P}\left(\frac{P \cdot h \cdot g(d)}{N_0 + I(\mathbf{z})} \geq T \right). \tag{2.42}$$

Assume network is interference-limited, i.e., $I(\mathbf{z}) \gg N_0$. Thus, noise is negligible. For calculation convenience, redefine scaled aggregate interference by

$$I(\mathbf{z}) = \sum_{\mathbf{x} \in \Phi'} h_X \cdot g(\mathbf{x}).$$

So the probability of successful transmission is

$$\begin{aligned}
\mathbb{P}_{suc}^{Full}(d, T) &= \mathbb{P}\left(\tfrac{h \cdot g(d)}{I(\mathbf{z})} \geq T \right) = \mathbb{P}\left(h \geq \tfrac{T I(\mathbf{z})}{g(d)} \right) \\
&= \int_0^\infty e^{-sT/g(d)} d\mathbb{P}(I(\mathbf{z}) \leq s) \\
&= L_{I(\mathbf{z})}(s)|_{s=T/g(d)},
\end{aligned} \tag{2.43}$$

where $L_X(s)$ is the Laplace transform function of random variable X, defined by $L_X(s) = \mathbb{E}[e^{-sX}]$.

As depicted in Eq.(2.43), successful transmission probability of the typical link in a full duplex network is based on Laplace function of inter-cluster aggregate interference $L_{I(\mathbf{z})}(s) = \mathbb{E}[e^{-sI(\mathbf{z})}]$. The Laplace function of inter-cluster aggregate interference is derived as follows:

$$
\begin{aligned}
L_I(s) = \mathbb{E}[e^{-sI(\mathbf{z})}] &= \mathbb{E}\left[e^{-s\left(\sum\limits_{\mathbf{x}\in\Phi'} h_X \cdot g(\mathbf{x})\right)}\right] \\
&= \mathbb{E}\left(\prod_{\mathbf{x}\in\Phi'} e^{-s\cdot h_X \cdot g(\mathbf{x})}\right) \\
&= \mathbb{E}_{\Phi'}\left(\prod_{\mathbf{x}\in\Phi'} \mathbb{E}_{h_X}[e^{-s\cdot h_X \cdot g(\mathbf{x})}]\right) \\
&= \mathbb{E}_{\Phi'}\left[\prod_{x\in\Phi'} v(s,\mathbf{x})\right],
\end{aligned}
$$

where $v(s,x) = \mathbb{E}_{h_X}[e^{-s\cdot h_X \cdot g(\mathbf{x})}] = \frac{1}{1+sg(\mathbf{x})}$, due to Rayleigh channel fading. Thus, Laplace function of inter-cluster aggregate interference is equal to generating functional $\mathcal{G}_{\Phi'}(v)$ of $v(s,\mathbf{x})$, i.e. $\mathbb{E}_{\Phi'}\left[\prod\limits_{\mathbf{x}\in\Phi'} v(s,\mathbf{x})\right]$.

The generating function of $v(s,\mathbf{x})$ of Thomas cluster process Φ' is given by [Stoyan et al. (1995)]

$$
\begin{aligned}
\mathcal{G}_{\Phi'}(v) &= \mathbb{E}\left(\prod_{\mathbf{x}\in\Phi'} v(s,\mathbf{x})\right) \\
&= \exp\left(-p\lambda_p \int_{\mathbb{R}^2}\left[1 - M\left(\int_{\mathbb{R}^2} v(s,\mathbf{x}+\mathbf{y})f(\mathbf{y})d\mathbf{y}\right)\right]d\mathbf{x}\right) \\
&= \exp\left(-p\lambda_p \int_{\mathbb{R}^2}\left[1 - \left(\int_{\mathbb{R}^2}\frac{1}{1+sg(\mathbf{x}-\mathbf{y})}f(\mathbf{y})d\mathbf{y}\right)^2\right]d\mathbf{x}\right)
\end{aligned}
\tag{2.44}
$$

where $M(n) = \sum\limits_{i=0}^{\infty} p_i n^i$ is the moment generating function of the number of points in the typical cluster. In this paper, there are two fixed points in the cluster, so $M(n) = n^2$. The last equation holds because $f(-\mathbf{y}) = f(\mathbf{y})$.

Combining E.q. (2.43) and E.q. (2.44), the successful transmission probability of full duplex

network is given by

$$
\begin{aligned}
\mathbb{P}_{suc}^{Full}(d,T) &= L_{I(\mathbf{z})}(s)|_{s=T/g(d)} \\
&= \exp\left(-p\lambda_p \int_{\mathbb{R}^2}\left[1-\left(\int_{\mathbb{R}^2}\tfrac{1}{1+Tg(\mathbf{x}-\mathbf{y})/g(d)}f(\mathbf{y})d\mathbf{y}\right)^2\right]d\mathbf{x}\right) \\
&= \exp\left\{-p\lambda_p \int_{\mathbb{R}^2}\left[1-\beta^2(\mathbf{x};d,T)\right]d\mathbf{x}\right\}
\end{aligned}
\tag{2.45}
$$

where $\beta(\mathbf{x};d,T) = \int_{\mathbb{R}^2}\frac{1}{1+Tg(\mathbf{x}-\mathbf{y})/g(d)}f(\mathbf{y})d\mathbf{y}$.

2.5 Successful Transmission Probability in Half Duplex Networks

In this section, successful transmission probability of half duplex with TDD slotted ALOHA is derived. Its equivalence with that of half duplex slotted ALOHA in Poisson point networks is proved. This result validates our framework of applying Thomas cluster point process to transmission capacity analysis.

2.5.1 Successful Transmission Probability

TDD slotted ALOHA is considered as the medium access control protocol when the radio is half duplex in Thomas cluster process. The transmitters form Thomas cluster process Φ_1 with one node in each cluster. The network density is $p\lambda_p$. Following the similar derivation in the full duplex communications, successful transmission probability of the typical link is Laplace function of inter-cluster aggregate interference $I_1(\mathbf{z})$. Hence, the successful transmission

probability of the typical link in a half duplex network is given by

$$
\begin{aligned}
\mathbb{P}_{suc}^{Half}(d,T) &= L_{I_1(\mathbf{z})}(s)|_{s=T/g(d)} \\
&= \exp\left(-p\lambda_p \int_{\mathbb{R}^2}\left[1-\left(\int_{\mathbb{R}^2}\frac{1}{1+Tg(\mathbf{x}-\mathbf{y})/g(d)}f(\mathbf{y})d\mathbf{y}\right)\right]d\mathbf{x}\right) \\
&= \exp\left\{-p\lambda_p \int_{\mathbb{R}^2}\left[1-\beta(\mathbf{x};d,T)\right]d\mathbf{x}\right\}
\end{aligned}
\tag{2.46}
$$

2.5.2　Equivalent Model of Half Duplex Transmission

Under the half duplex TDD scheme, the transmitters form Thomas cluster process with one point in each cluster. We prove in Theorem 2 that the network point process is equivalent to Poisson point process with the same network density.

Theorem 2.4. *Let Φ_1 be the Thomas cluster process with one point in each cluster, the density of virtual parent point process of Φ_1 be λ_p, and Φ_2 be Poisson point process with density λ_p. Then, Φ_1 and Φ_2 are equivalent with the same spatial distribution.*

Proof. In the Thomas cluster process Φ_1, the virtual parent point process is Poisson point process with density λ_p, and the one cluster point is placed around its virtual parent point with the normal distribution, and the distribution function, as showed in E.q. (2.1), only depends on $(\mathbf{y}-\mathbf{x})$. According to the displacement theorem [Martin (2012)], treating the virtual parent point process as the original process, the one cluster point process as the displaced point process, the displaced point process is also Poisson with the same density, i.e. Thomas cluster process Φ_1 is also Poisson point process with the same density. Thus, Φ_1 and Φ_2 are equivalent with the same spatial distribution. □

In Poisson point network with density λ_p, successful transmission probability $\mathbb{P}_{suc}(d,T)$ of the typical link in half duplex communications is given by [Weber et al. (2005)]

$$
\begin{aligned}
\mathbb{P}_{suc}(d,T) &= \exp\left\{\lambda_p \int_{\mathbb{R}^2}\left[1-v(s,\mathbf{x})|_{s=T/g(z)}\right]d\mathbf{x}\right\} \\
&= \exp\left(-\lambda \int_{\mathbb{R}^2}\left(1-\frac{1}{1+Tg(\mathbf{x})/g(d)}\right)d\mathbf{x}\right).
\end{aligned}
\tag{2.47}
$$

After the slotted ALOHA protocols, successful transmission probability $\mathbb{P}_{suc}(d, T)$ of the typical link in half duplex Posson point network is given by

$$\mathbb{P}_{suc}(d, T) = \exp\left(-p\lambda_p \int_{\mathbb{R}^2} \left(1 - \frac{1}{1+Tg(\mathbf{x})/g(d)}\right) d\mathbf{x}\right). \tag{2.48}$$

According to E.q. (2.46), in the Thomas cluster point process with one point in each cluster and density λ_p, after slotted ALOHA, successful transmission probability $\mathbb{P}_{suc}^{Half}(d, T)$ of the typical link in half duplex Thomas cluster network is given by

$$
\begin{aligned}
\mathbb{P}_{suc}^{Half}(d, T) &= \exp\left\{-p\lambda_p \int_{\mathbb{R}^2} \left[1 - \beta(\mathbf{x}; d, T)\right] d\mathbf{x}\right\} \\
&= \exp\left(-p\lambda_p \int_{\mathbb{R}^2} \left[\int_{\mathbb{R}^2} \left(1 - \frac{1}{1+Tg(\mathbf{x}-\mathbf{y})/g(d)}\right) f(\mathbf{y}) d\mathbf{y}\right] d\mathbf{x}\right) \\
&= \exp\left(-p\lambda_p \int_{\mathbb{R}^2} \left(1 - \frac{1}{1+Tg(\mathbf{x})/g(d)}\right) d\mathbf{x}\right)
\end{aligned}
\tag{2.49}
$$

Comparing E.q. (2.48) and E.q. (2.49), we can get

$$\mathbb{P}_{suc}^{Half}(d, T) = \mathbb{P}_{suc}(d, T).$$

Thus, our analysis based on Thomas cluster point process achieves the same result from the Poisson point process.

To simplify the derivation results later on, let

$$
\begin{cases}
\alpha^H(d, T) &= \int_{\mathbb{R}^2} \left[1 - \beta(\mathbf{x}; d, T)\right] d\mathbf{x} \\
\alpha^F(d, T) &= \int_{\mathbb{R}^2} \left[1 - \beta^2(\mathbf{x}; d, T)\right] d\mathbf{x}
\end{cases}
$$

Lemma 2.1. $\alpha^H(d, T) \leq \alpha^F(d, T) \leq 2\alpha^H(d, T), \forall T, d \in \mathbb{R}^+$.

Proof. From the form of $\beta(\mathbf{x}; d, T)$, we can know that

$$\beta(\mathbf{x}; d, T) \leq 1, \forall \mathbf{y} \in \mathbb{R}^2, d \in \mathbb{R}^+.$$

moreover,

$$1 - \beta^2(d, \mathbf{x}; T) = (1 - \beta(d, \mathbf{x}; T))(1 + \beta(d, \mathbf{x}; T)).$$

Thus we know that

$$\alpha^H(d, T) \leq \alpha^F(d, T) \leq 2\alpha^H(d, T), \forall T, d \in \mathbb{R}^+.$$

$\square$

2.6   Transmission Throughput and Transmission Capacity

Transmission throughput, which represents mean throughput in a unit network area, is defined for both full duplex and half duplex random wireless network. If the transmission link density is λ, then the transmission throughput (TH) is defined as

$$TH(d, T) = \lambda \log(1 + T)\mathbb{P}_{suc}(d, T),$$

where T is the SINR threshold, and $\mathbb{P}_{suc}(d, T)$ is the successful transmission probability for the typical link with distance d. E.q (2.45) and E.q (2.46) are the formula results of $\mathbb{P}_{suc}(d, T)$ for full duplex communications and half duplex communications respectively. In this paper, the transmission link density is $p\lambda_p$ for half duplex network, while in full duplex network, the transmission link density is $2p\lambda_p$.

Transmission capacity is another network metric, which is defined as the maximum transmission throughput, subject to a constraint on the transmission outage probability of the typical link. Let ϵ be the outage probability constraint of the typical link, i.e. $\mathbb{P}_{out}(d, T) = 1 - \mathbb{P}_{suc}(d, T) \leq \epsilon$. Then the transmission capacity is defined as

$$TC(d, \epsilon) = \max_{(\lambda, T):\mathbb{P}_{out} \leq \epsilon} \lambda \log(1 + T)(1 - \epsilon), \tag{2.50}$$

where λ is the transmission link density.

E.q. (2.50) is a two-dimensional optimization problem. Instead of getting an optimal result for both λ and T, we are more intested in the optimal result when either λ or T is fixed. When node density λ is fixed,we have the following capacity:

$$TC(d, \lambda_p, \epsilon) = \begin{cases} \max\limits_{T: \mathbb{P}_{out}^{half} \leq \epsilon} p\lambda_p (1 - \epsilon) \log(1 + T), & \text{Half Duplex} \\ \max\limits_{T: \mathbb{P}_{out}^{full} \leq \epsilon} 2p\lambda_p (1 - \epsilon) \log(1 + T), & \text{Full Duplex.} \end{cases} \tag{2.51}$$

When transmission rate is fixed, we have following capacity:

$$TC(d, T, \epsilon) = \begin{cases} \max\limits_{\lambda_p: \mathbb{P}_{out}^{half} \leq \epsilon} p\lambda_p (1 - \epsilon) \log(1 + T), & \text{Half Duplex} \\ \max\limits_{\lambda_p: \mathbb{P}_{out}^{full} \leq \epsilon} 2p\lambda_p (1 - \epsilon) \log(1 + T), & \text{Full Duplex.} \end{cases} \tag{2.52}$$

In this case, the transmission capacity can be derived in closed-forms.

$$TC(d, T, \epsilon) = \begin{cases} \frac{(1-\epsilon)\ln(1-\epsilon)\log(1+T)}{\alpha^H(d,T)}, & \text{Half Duplex} \\ \frac{2(1-\epsilon)\ln(1-\epsilon)\log(1+T)}{\alpha^F(d,T)}, & \text{Full Duplex.} \end{cases} \tag{2.53}$$

From Lemma.1, we can conclude that

$$TC^{Half}(d, T, \epsilon) \leq TC^{Full}(d, T, \epsilon) \leq 2TC^{Half}(d, T, \epsilon). \tag{2.54}$$

2.7 Numerical Results

In this section, numerical results are presented on transmission throughput and transmission capacity of half duplex and full duplex wireless networks. A few common parameters are fixed throughout the numerical simulations and given as follows. In normal distribution function,
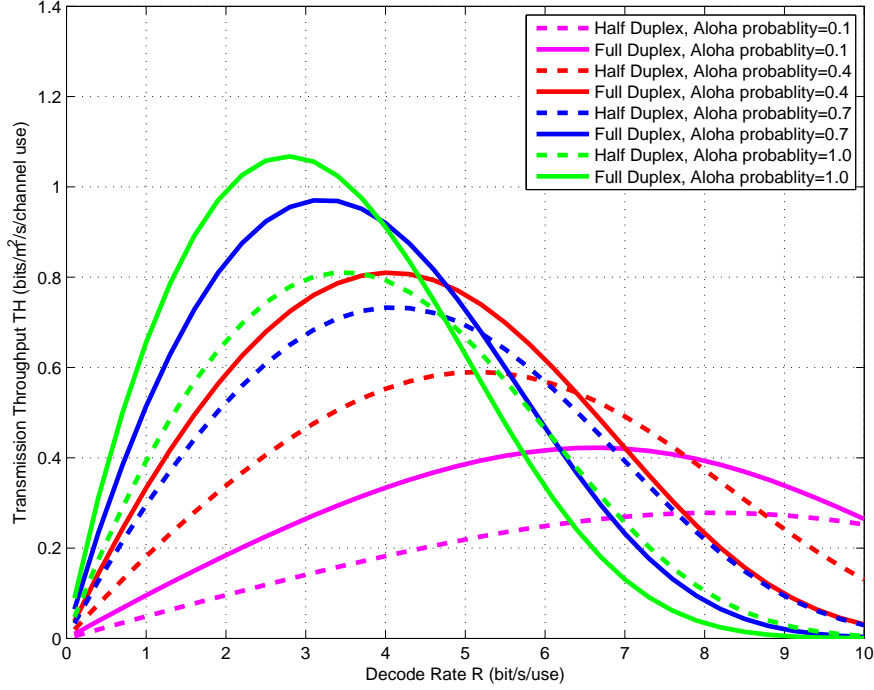
Figure 2.3: Transmission throughput of full duplex and half duplex communications.

the variance $\sigma^2 = \frac{1}{16}$. The path-loss function is $g(\mathbf{x}) = \frac{a^\alpha}{\|\mathbf{x}\|^\alpha}$ with $\alpha = 4$ and $\|x\| \geq a$, while $a = 0.125m$ represents the wavelength of the electric wave. Typical link distance is set to be the mean value,i.e. $\sqrt{\pi}\sigma$.

2.7.1   Transmission Throughput

In Fig. 2.3, transmission throughput of half duplex and full duplex communications are shown by solid lines and dash lines, respectively, under the slotted ALOHA protocol with four transmission probabilities $p = 0.1, 0.4, 0.7, 1.0$. Network density is $2\lambda_p = 1.0$.

Given fixed transmission probability p, transmission throughput increases in the low transmission rate region, reaches a saturation point at a certain transmission rate R_s, and then decreases in the high transmission rate region for both half duplex and full duplex communications. The reason is that transmission links can tolerate high aggregate interference in the low

transmission rate region. Then, the advantage of full duplex communications, i.e. the number of active transmitters is twice as many as that in half duplex communications, is well taken. Thus, full duplex communications outperform half duplex communications in the low transmission rate region. In the high transmission rate region, transmission link can only tolerate low aggregate interference. Then, the advantage of half duplex, i.e. less interference experienced by a link, is more dominant. Thus, half duplex communications outperform full duplex communications in the high transmission rate region.

Results in Fig. 2.3 also show that a higher transmission probability p leads to lower saturation transmission rate R_s, e.g. $p = 0.1$, $R_s = 8.7$ bit/s/use, $p = 0.4$, $R_s = 5.3$ bit/s/use in full duplex communications, and $p = 0.7$, $R_s = 3.2$ bit/s/use, $p = 1.0$, $R_s = 2.8$ bit/s/use in half duplex communications. The reason is that a higher transmission probability results in more active transmitters in the network, making the network reach the saturation state at a lower transmission rate. For the same transmission probability p, the full duplex transmission throughput is larger than that of half duplex system in the low transmission rate region, but lower in the high transmission rate region.

Transmission throughput ratio between full duplex and half duplex communications is shown in Fig. 2.4. Similar to Fig.2.3, transmission throughput ratio decreases from almost 2 to 0 as transmission rate increases for each probability p. Define the point R_t as the transmission rate where the full duplex transmission throughput is equal to half duplex transmission throughput. As shown in Fig. 2.4, R_t decreases as transmission probability p increases, e.g. R_t equals to 10.2, 6.6, 5.1, 4.8 bit/s/use for $p = 0.1$, 0.4, 0.7, 1.0. It reflects the fact that a higher transmission probability p introduces more active transmitters, making R_t be located at lower transmission rate where the full duplex transmission throughput and the half duplex transmission throughput are equal.
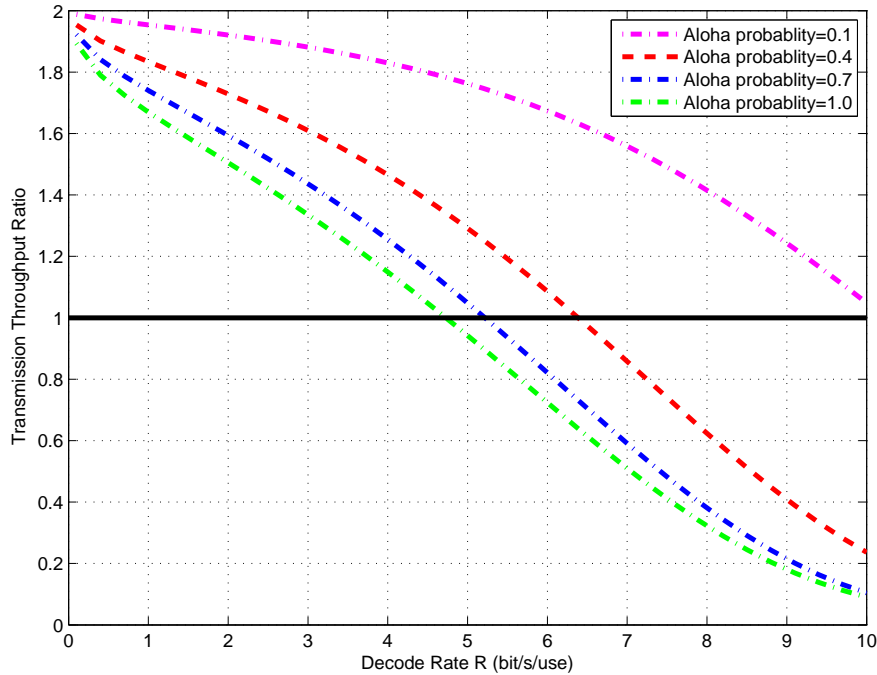
Figure 2.4: Transmission throughput ratio between full duplex and half duplex under different ALOHA probability.

2.7.2   Transmission Capacity

Transmission capacity is defined as maximum transmission throughput under an outage probability constraint. Here, outage probability constraint is set to be $\epsilon = 0.02$.

(1) Transmission Capacity under Optimal Transmission Rate and Fixed Network Density

Network topology is the same for half duplex and full duplex communications, and network throughput is maximized by optimizing the transmission rate to get transmission capacity. To show different transmission capacity versus network density, network density varies from 0.0001 to 0.30.

The maximum transmission rates for half duplex communications and full duplex communications are shown in Fig. 2.5. As the network density increases, the transmission rate decreases
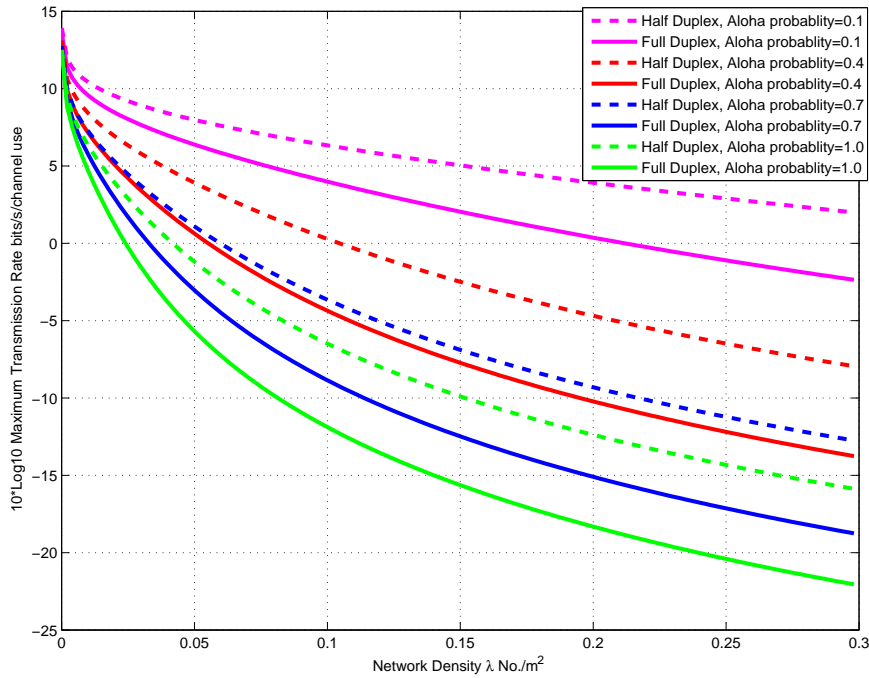
Figure 2.5: Transmission rate of full duplex and half duplex under different network density requirement.

in both half duplex and full duplex communications, because a higher network density causes more aggregate interference. Because there exist more transmissions in full duplex communication under the same network density, aggregate interference in full duplex communications is more severe than that in half duplex communications. To tolerate the severe interference, the maximum transmission rate in full duplex communications is lower than that in half duplex communications. As shown in Fig. 2.5, the gap between maximum transmission rates in half duplex and full duplex communications becomes larger as network density increases.

In Fig. 2.6, half duplex and full duplex transmission capacities are shown. As the network density increases, the co-channel interference also increases. In the low network density region, interference is very limited in the network. Moreover, increasing network density provides more transmissions. Thus the transmission capacity increases as network density increases in the low network density region. However, in the high network density region, severe aggregate
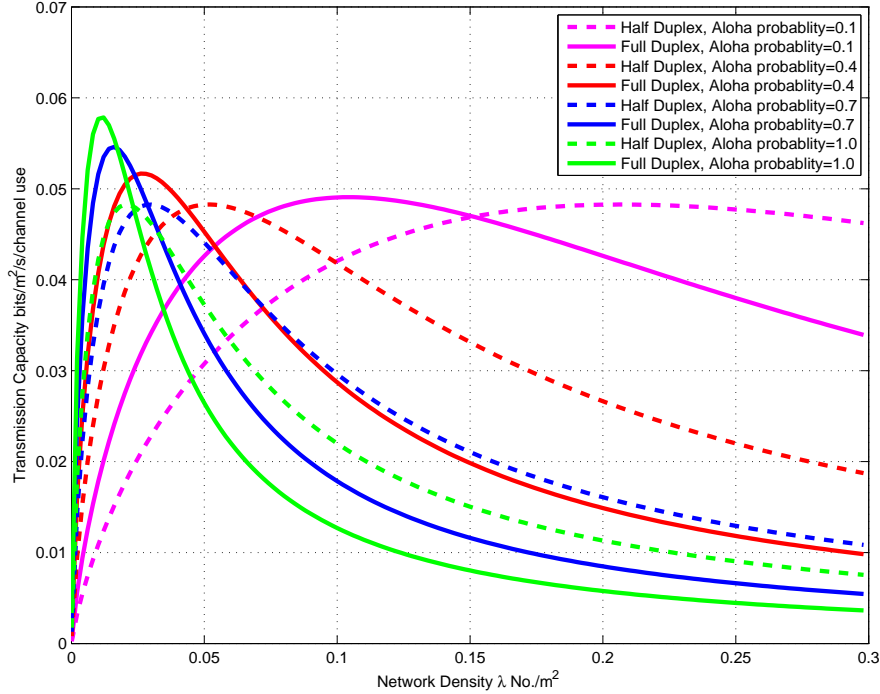
Figure 2.6: Transmission capacity of full duplex and half duplex under different network density requirement.

interference gradually reduces the transmission rate, resulting in the decrease of transmission capacity. Moreover, considering the point λ_p^t as the network density where the full duplex transmission throughput is equal to the half duplex transmission capacity, λ_p^t also decreases as transmission probability p increases. For example, λ_p^t equals to 0.150, 0.046, 0.035, 0.026 for $p = 0.1, 0.4, 0.7, 1.0$. The reason is that a higher transmission probability p means more active transmitters, making λ_p^t be located at lower network density where full duplex and half duplex transmission throughput are equal.

As shown in Fig. 2.7, the transmission capacity ratio between full duplex and half duplex communications decrease from 2 to a number less than 0.6 as network density increases. It indicates that, under a fixed network density, full duplex communications outperforms half duplex only in the low network density region, but lose the advantage in the high network density region.
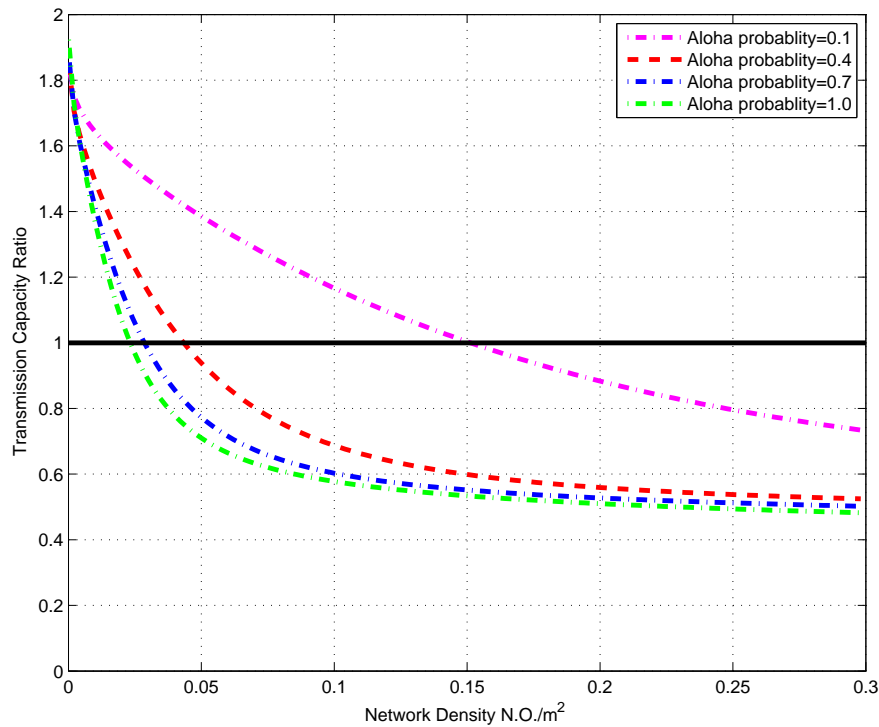
Figure 2.7: Transmission capacity ratio between full duplex and half duplex under different network density requirement.

(2) Transmission Capacity under Optimal Network Density and Fixed Transmission Rate

The transmission rate is fixed and the same for half duplex and full duplex communications. The transmission throughput is maximized by varying the network density to reach transmission capacity.

The maximum network density for full duplex and half duplex communications are shown in Fig. 2.8. Results show that, under the same transmission probability p, a higher transmission rate can be satisfied at a lower network density. In Fig. 2.9, transmission capacity under different transmission probability is shown for both half and full duplex communications. The trends of this case is similar to that of transmission capacity versus transmission rate under a
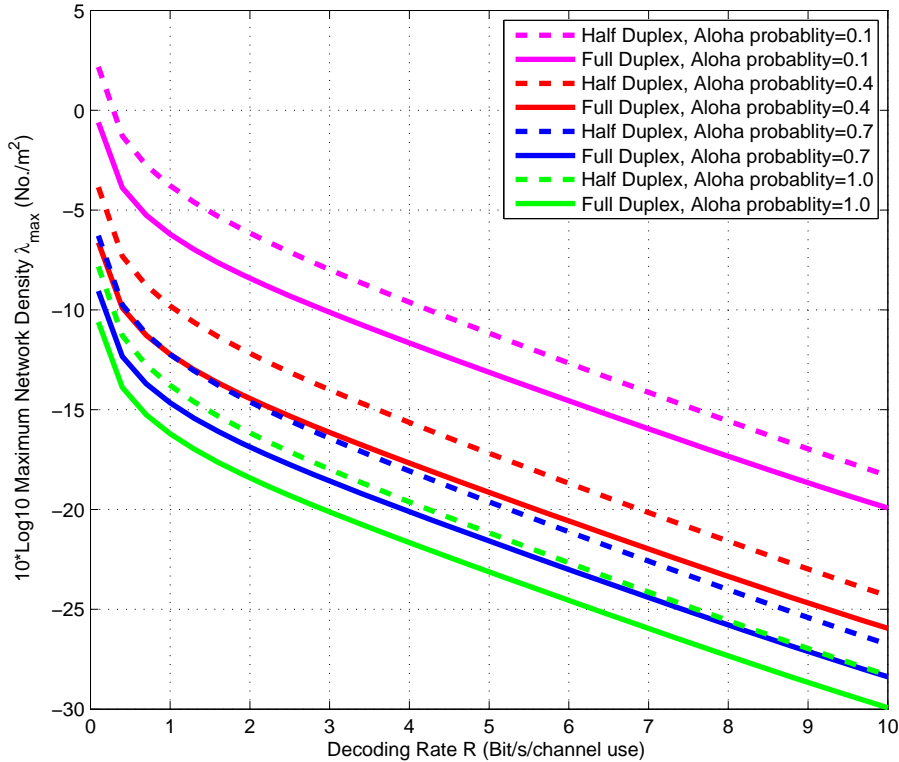
Figure 2.8: Network density of full duplex and half duplex under different transmission rate.

fixed network density.

For both half duplex and full duplex communications, if the network is in the low transmission rate region, then the optimized network density is very high, because nodes can tolerate high interference. However, due to low transmission rate, the overall transmission capacity is low. When the network is in the high transmission rate region, then the network density is very low, which also makes the overall transmission capacity low. As a result, when the transmission rate increases from the low region to the high region, the transmission capacity increases at first and then decreases. In other words, there exists an optimal point of the network density to achieve the maximum transmission capacity.

Different from transmission capacity under a fixed network density, transmission capacity in this case does not change with a different transmission probability p. The reason is that the
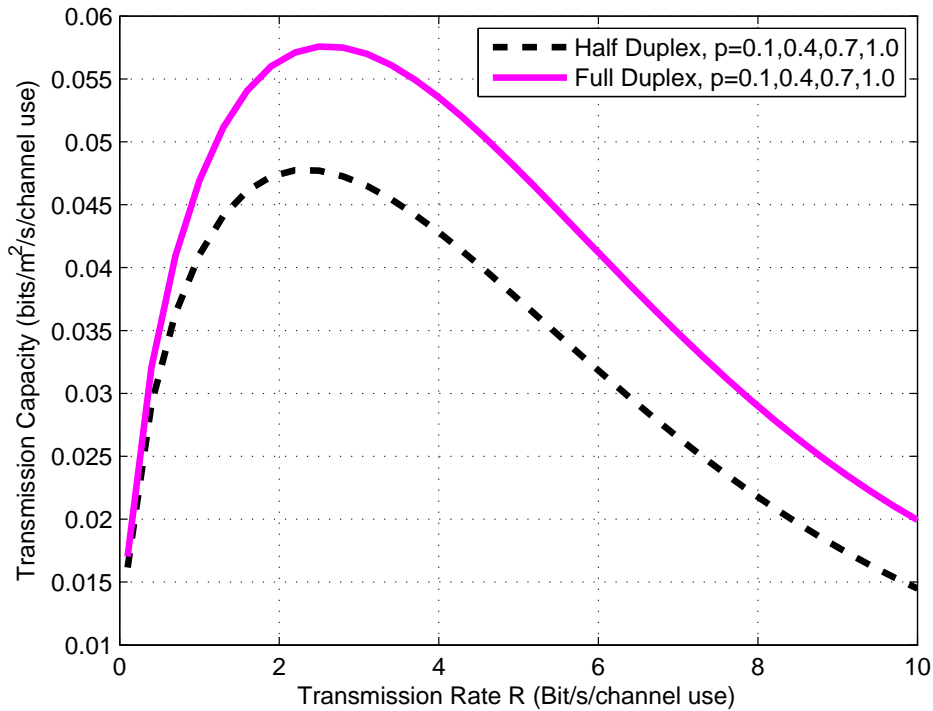
Figure 2.9: Transmission capacity of full duplex and half duplex under different transmission rate.

maximum density of active transmitters that the network can support keeps unchanged with different transmission probabilities p. For a different transmission probability, the network density is optimized to reach the same maximum number of active transmitters to achieve the transmission capacity under a fixed transmission rate. Thus, transmission probability does not affect transmission capacity in full duplex and half duplex communications in this case.

Based on results in Fig. 2.9, the transmission capacity ratio is depicted in Fig. 2.10. We find that the transmission capacity of full duplex communication is always larger than that of half duplex communication under the same transmission rate requirement. Moreover, transmission capacity ratio varies from 1.00 to 1.38, indicating that the network capacity gain from full duplex communications is limited in large scale networks.
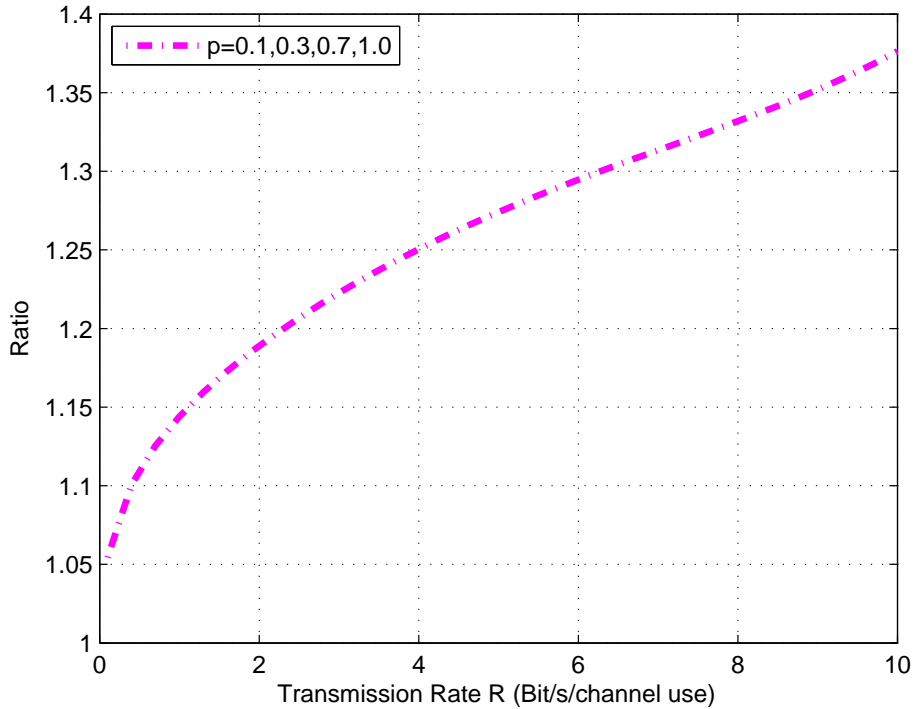
Figure 2.10: Transmission capacity ratio between full duplex and half duplex under different transmission rate.

2.8   Summary

In this chapter, the aggregate interference and transmission capacity of a full duplex wireless network were derived via stochastic geometry, and comparisons with half duplex communications were conducted to present one solution to how much network throughput gain full duplex communications can bring. The network topology was set to follow Thomas cluster point process with two daughter point in each cluster, and full duplex and half duplex Slotted ALOHA medium access control protocols were fixed to fit for half and full duplex communications. It is prove that the half duplex communication with network topology of Thomas cluster point process is equal to commonly used half duplex communication with network topology of Poisson point process. Analytical results show the close-form derivation for the mean and variance of aggregate interference in full duplex networks and the upper and lower bounds for the aggregate

interference's tail probability for both half and full duplex networks. The asymptotic order of aggregate interference's tail probability was proved be the same for both half and full duplex communication networks, which leads to more dispersal aggregate interference distribution in full duplex networks than in half duplex networks. Then, two definition of transmission capacity, including commonly used transmission capacity, were derived to measure the maximum network throughput in both half duplex and full duplex communication networks.

Numerical results showed that, under the conditions of the same network density and the transmission rate with outage constraint, transmission throughput of full duplex wireless networks outperforms that of half duplex wireless networks in low transmission rate region. However, the performance of full duplex wireless networks is lower in high transmission rate region. The transmission capacity gain in full duplex communications is limited, as revealed from analytical results. The major reason behind this issue is that the aggregate interference is severe in full duplex communications. This issue indicates the importance of developing mutual-interference cancelation techniques for full duplex communications. Capacity analysis considering both self-interference and mutual-interference cancelation is also an interesting topic for future work.

Chapter 3

Full Duplex Cellular Network and Mutual-interference Cancelation

In this chapter, average rate and coverage probability of typical uplink and downlink are presented in a full duplex cellular network . Consider FDR mode on base stations for full duplex communication. Mutual interference cancelation technique is put forward and assumed to conduct between uplink transmission pairs via functionality of base stations. Two-layer Poisson point process is proposed to model the network topology. Properties of Poisson point process are utilized to derive the aggregate interference for both typical uplink and downlink. For both typical uplink and downlink, comparisons of average rate and coverage probability between the half duplex cellular network and the full duplex cellular network with/without mutual interference cancelation are presented.

3.1 Motivation

3G and 4G cellular networks has been widely deployed to meet rapidly increased mobile communication demands. New network structures and physical techniques are proposed to improve network spectrum efficiency. Emerging full duplex wireless communication is one of these
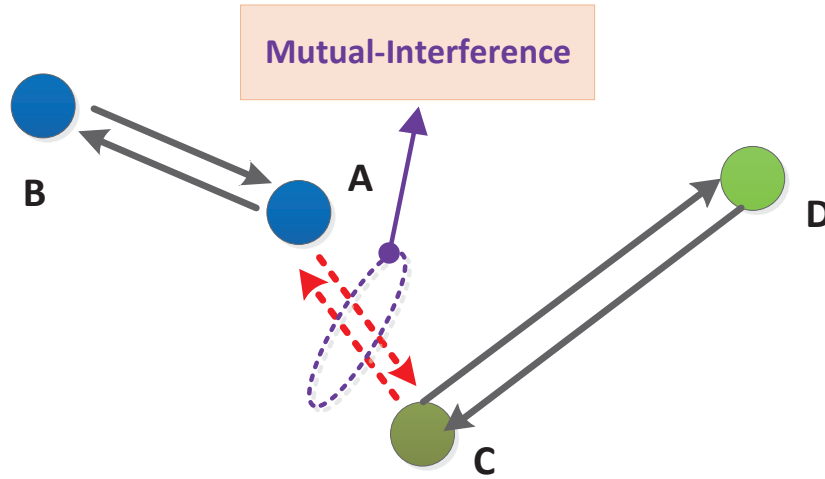
Figure 3.1: Mutual interference in full duplex communication networks.

promising techniques that have the potential to increase capacity of cellular networks. It is still an open research problem on how much network capacity gain full duplex communication can be obtained in cellular networks.

Theoretically, full duplex communication can double the link throughput due to the feasibility of simultaneous transmission and reception in the same frequency. But it is hard to determine the network capacity gain of full duplex communications in cellular networks. Different from wireless ad hoc networks, cellular networks have relatively stable structure, which is dominated by base stations. Full duplex communication technique introduces more transmission links, thus causes severe aggregate interference with high probability, which is confirmed in [Wang and Huang (2014)]. One of the key reasons is severe mutual interference between full duplex communication pairs in the wireless networks, depicted in Fig. 3.1. Node A and B, C and D are two full duplex communication pairs. A and C are too closed and cause mutual interference to each other, labeled by red dash line.

To combat severe mutual interference problem in full duplex communication networks, two
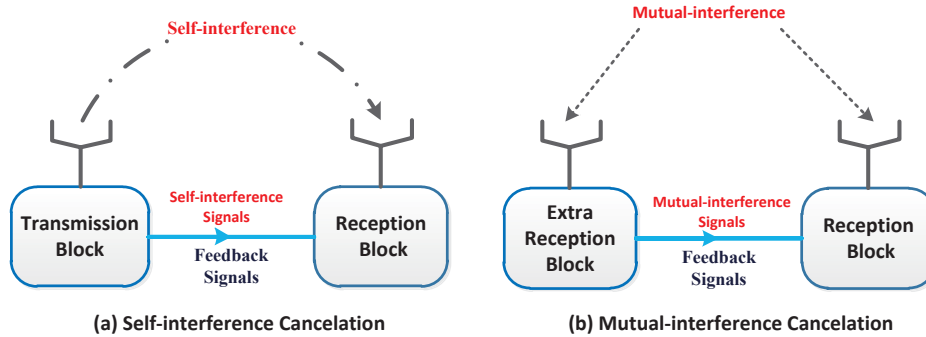
Figure 3.2: Self interference cancelation mechanism V.S. mutual interference cancelation mechanism.

main approaches are put forwards, interference avoidance and interference cancelation. Interference avoidance is mostly implemented by proper medium access control(MAC) protocols, such as Contraflow in [Radunovic et al. (2009)] and FD-MAC in [Kim and Stark (2013)]. On the other hand, interference cancelation can be done by the same mechanisms as self-interference cancelation techniques. The system requirement is that the mutual interference nodes know each other's transmitting signals. Name such cancelation technique as mutual interference cancelation (MIC) techniques, showed in Fig. 3.2. Acquisition of the mutual interference signal can be implemented by both wire and wireless communication techniques, such as signal feedback via optical fiber, or directional antennas [Ramanathan et al. (2005)] over the air, which is not the focus of this thesis. Thus, another target of this chapter is to analyze how much network capacity gain of full duplex communication can be improved by mutual interference cancelation in the cellular network.

The key challenges to study network capacity gain of full duplex communication cover following two aspects, how to choose the full duplex communication mode and model complicated aggregate interference on typical uplink and downlink in cellular networks. For the first challenge, we adopt a simplified version of full duplex cellular network with full duplex radios installed on base stations to exploit, and FDR mode is chosen for uplink and downlink trans-

mission. As for the aggregate interference, there exit two approaches to present closed-form derivation. The first approach is traditional fixed topology model, in which cellular networks are modeled by placing the base stations according to a regular geometry, such as Wyner model, hexagonal grid. However, these highly idealized models are far from accurate in terms of interference and capacity [Xu et al. (2011)]. The second approach is General models based on stochastic geometry for cellular networks by assuming that base stations and/or mobile users follow a certain spatial point process, such as Poisson Point Process [Martin et al. (2009)].

We adopt two-layer Poisson point process as the network topology to model uplink mobile users and base stations in full duplex cellular network. Due to the stable network structure, uplink and downlink distances are affected by network topology in cellular networks, whose distribution is calculated via property of Poisson point process. The aggregate interference is modeled as shot-noise process with careful consideration on interferers' distributions in the network. Tools from stochastic geometry are used to derive closed-form aggregate interference model.

Network capacity is measured by coverage probability of the typical uplink and downlink, defined by the probability that the link state achieve target SINR requirement T. Thus, it represents the probability that a randomly chosen user can receive information bits successfully. Due to the random network topology model, coverage probability also represents the mean fraction of area in successful reception pattern, i.e. the average fraction of wireless terminals which achieve target SINR requirement T at any time, i.e. $\mathbb{P}_c(T) = \mathbb{P}(SINR > T)$. Based on coverage probability, average rate of the typical link is derived, which represents mean data rate that are achievable for a cellular network cell.

$$\bar{R} = \mathbb{E}[\log_2(1+T)] = \int\limits_0^\infty \log_2(1+T)d(1-\mathbb{P}_c(T))dT. \tag{3.1}$$

The rest of this chapter is organized as follows. System models are described in Section 3.2.

Coverage probability of downlink and uplink in the half duplex cellular network are derived in Section 3.3, while Section 3.4 presents coverage probability of downlink and uplink in the full duplex cellular network. Mutual interference cancelation's effect on coverage probability is analyzed in Section 3.5. At last, numerical results are plotted and discussion on network capacity gain of full duplex communications with/without mutual interference cancelation are presented in Section 3.6. The chapter is summarized in Section 3.7.

3.2   System Model

In this section, transmission schemes, network topology model, and physical layer setting are introduced for half and full duplex cellular networks.

3.2.1   Transmission Schemes

Single channel transmission schemes are considered in both half duplex and full duplex cellular networks. Under half duplex communication condition, Time Duplex Division (TDD) transmission scheme [Esmailzadeh and Nakagawa (2003)] is adopted for uplink and downlink transmissions, i.e. downlink and uplink transmissions take turns to be activate in half duplex communication cellular network. For full duplex communication, full duplex radios are assumed to install on the base stations, while all mobile users have traditional half duplex radios. Then, full duplex base stations make it reality to operate uplink and downlink transmission simultaneously in a single channel. Assume every base station always has one downlink mobile user and one uplink mobile user to serve.

Intuitively, full duplex communication introduces more aggregate interference for both uplink and downlink transmission in the cellular network. Considering the powerful functionality of base stations, mutual interference cancelation can be conducted at the base stations. When mutual interference cancelation is conducted in full duplex communication cellular network,
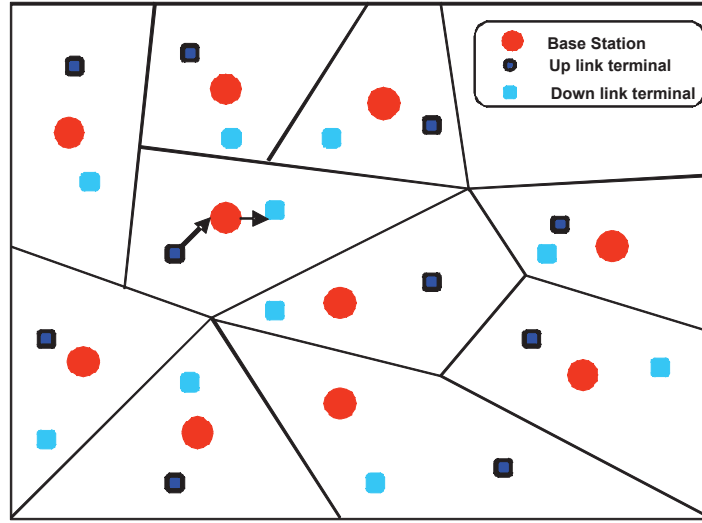
Figure 3.3: Cellular networks structure.

the aggregate interference from concurrent transmissions of base stations is canceled. It can be concluded easily that mutual interference cancelation at the base stations only improves the uplink data transmission. We assume that perfect cancelation is planed to explore, where the aggregate interference from all base stations are canceled completely.

3.2.2   Network Topology Model

A two-layer spatial point process is used to model cellular network topology. At first, a homogeneous Poisson point process (PPP) Φ_B with density λ is modeled as the spatial distribution of base stations. Then, the two dimensional space is divided into Voronoi cells, which form Voronoi Tessellation [Stoyan et al. (1995)]. To model our single channel transmission schemes, one active uplink mobile user and downlink mobile user lies in each cell, depicted in Fig. 3.3. As for the downlink transmission in the half duplex cellular network, a mobile user is assumed to locate at origin, and it is treated as the typical receiver. The typical transmitter is the base station associated with typical mobile users. All active transmitting terminals are base stations, which form Poisson point process. As for the uplink transmission in the half duplex

cellular network, a base station is assumed to locate at origin, and it is treated as the typical receiver. All the active transmitting terminals are uplink mobile users, which is also assumed to be Poisson point process (PPP) Φ_U with density λ_u. Due to the single channel communication assumption, the density of uplink mobile users is equal to density of mobile stations, i.e. $\lambda_u = \lambda$.

In full duplex cellular networks, the active transmitting terminals include both uplink mobile users and base stations, which are modeled by a two-layer Poisson point process. Poisson point process Φ_B is for base stations while Φ_U is for uplink mobile users. Since there is only one base stations and uplink mobile that can be active in single channel full duplex cellular network, both Poisson point process have the same density λ. Moreover, the locations of mobile users and base stations are correlated, thus, careful attentions are called when calculating the aggregate interference from both active mobile users and base stations.

3.2.3   Physical Layer setting

Assume that all base stations transmit with the same power P_B, while all the mobile users transmit with the same power P_U. The channel bandwidth is B and the background noise W is Gaussian with power spectrum density $\frac{N_0}{B}$. Hence, the received noise power is N_0. To model signal propagation through wireless channels, two types of fading are considered: small scale fading and large fading. Rayleigh channel fading with unit mean captures small scale fading, while large-scale fading is described by a path-loss attenuation model [Ganti and Haenggi (2009)], represented as path loss attenuation function $g(\mathbf{x}) : \mathbb{R}^2 \to \mathbb{R}^+$. The most common used forms of $g(\mathbf{x})$ are $\|\mathbf{x}\|^{-\alpha}$, $(1 + \|\mathbf{x}\|^\alpha)^{-1}$, and $\min\{1, \|\mathbf{x}\|^{-\alpha}\}$, among which the first one is chosen as the path loss attenuation model in this chapter.

Thus, if a transmitter X at location $\mathbf{x}$ tries to send symbols to receiver Y at location $\mathbf{y}$, the received power at Y is $P \cdot h_{XY} \cdot g(\mathbf{y} - \mathbf{x})$, where P is the transmitting power, h_{XY} is the power fading coefficient associated with the wireless channel between terminal X and Y, and

$g(\mathbf{x}) : \mathbb{R}^2 \to \mathbb{R}^+$ is the path loss attenuation function. For the link transmission, successful transmission occurs only if the link signal-interference plus noise ratio (SINR) is above a fixed threshold T. According to the Shannon Capacity theorem [Shannon (2001)], the SINR threshold T is determined by the rate requirement of the cellular network.

3.3   Coverage Probability in the Half Duplex Cellular Network

In this section, coverage probability of the typical link for downlink and uplink communications in half duplex cellular network is presented, defined as the probability of the typical link's successful transmission, i.e. the typical link's SINR is above a fixed threshold T. Hence, coverage probability of the typical link is expressed as $\mathbb{P}_c(T) = \mathbb{P}[SINR \geq T]$.

Considering the downlink transmission, the typical receiving mobile user u_0 is assumed to place at the origin of the plane, and the typical transmitting base station is denoted as b_0. Under the topology setting, base station b_0 is the nearest base station to the mobile user u_0. The downlink typical link's SINR_D^H is expressed as

$$SINR_D^H = \frac{P_B h_0 r^{-\alpha}}{N_0 + I_r^{\Phi_B}}, \tag{3.2}$$

where $r = \|b_0\|$ is the link distance, h_0 is the power of rayleigh fading channel between b_0 and u_0, and $I_r^{\Phi_B}$ is the aggregate interference from concurrent downlink transmissions of base stations, described as

$$I_r^{\Phi_B} = \sum_{\mathbf{x} \in \Phi_B / b_0} P_B h_{\mathbf{x}} \|\mathbf{x}\|^{-\alpha}. \tag{3.3}$$

Note that all the channels $\{h_{\mathbf{x}} : \mathbf{x} \in \Phi_B\}$ are Rayleigh fading with unit mean.

Due to the Poisson point process deployment of base stations, the link distance r is a random variable. Its probability density function (PDF) is derived in following lemma [Andrews et al.

(2011)].

Lemma 3.1. *The probability density function of link distance r is $f_r(t) = 2\pi\lambda t e^{-\pi\lambda t^2}$.*

Proof. Since b_0 is the nearest base station to typical receiving mobile user u_0, no base station lies in the region $\Omega(o, t) := \{\mathbf{x} \in \mathbb{R}^2 : \|\mathbf{x}\| \leq t\}$. Thus, we get

$$\begin{aligned}
\mathbb{P}[r \leq t] &= 1 - \mathbb{P}[r > t] \\
&= 1 - \mathbb{P}[\Phi(\Omega(o, r)) = \emptyset] \\
&\stackrel{(a)}{=} 1 - e^{-\lambda\pi t^2},
\end{aligned}$$
(3.4)

where equality (a) is due to the property of Poisson point process. Hence, the probability density function of link distance r is $f_r(t) = \frac{df_r(t)}{dt} = 2\pi\lambda t e^{-\pi\lambda t^2}$. □

Tools from stochastic geometry are employed to derive the downlink coverage probability, which is showed in following theorem [Andrews et al. (2011)].

Theorem 3.1. *The downlink coverage probability of the typical link in half duplex cellular network is*

$$\mathbb{P}_c^{HD} = \int\limits_0^\infty 2\pi\lambda r \exp\left(-\frac{Tr^\alpha N_0}{P_B} - \lambda\pi r^2 \rho(T, \delta)\right) dr,$$
(3.5)

where $\rho(T, \delta) = \frac{1}{1+T} + \mathbb{E}_h[(Th)^\delta(\Gamma(1 - \delta) - \Gamma(1 - \delta, Th)]$ with h following unit exponential distribution, $\Gamma(x) = \int_0^\infty t^{x-1} e^{-t} dt$ is the Gamma function and $\Gamma(x, z) = \int_z^\infty t^{x-1} e^{-t} dt$ is the incomplete Gamma function.

Proof. By definition of conditional probability, the downlink coverage probability is expressed

as

$$
\mathbb{P}_c^{HD} = \mathbb{E}_r[\mathbb{P}[SINR_D^H > T|r]]
$$

$$
= \int_0^\infty \mathbb{P}[SINR_D^H > T|r]f_r(r)dr
$$

$$
\overset{(a)}{=} \int_0^\infty \mathbb{P}[h_0 > \frac{Tr^\alpha(N_0 + I_r^{\Phi_B})}{P_B}]f_r(r)dr. \tag{3.6}
$$

Equality (a) results from substitution of E.q. (3.12). Due to Rayleigh channel fading with unit mean, h_0 follows unit exponential distributions. Thus

$$
\mathbb{P}[h_0 > \frac{Tr^\alpha(N_0 + I_r^{\Phi_B})}{P_B}] = \mathbb{E}_{\Phi_B}\left[\mathbb{P}[h_0 > \frac{Tr^\alpha(N_0 + I_r^{\Phi_B})}{P_B}|\Phi_B]\right]
$$

$$
= \mathbb{E}_{\Phi_B}\left[\exp\left(-\frac{Tr^\alpha(N_0 + I_r^{\Phi_B})}{P_B}\right)|\Phi_B\right] \tag{3.7}
$$

$$
= \exp\left(-\frac{Tr^\alpha N_0}{P_B}\right) L_{I_r^{\Phi_B}}\left(\frac{Tr^\alpha}{P_B}\right),
$$

where $L_{I_r^{\Phi_B}}(s)$ is the Laplace transformation of random variable $I_r^{\Phi_B}$ evaluated at s. By substituting E.q. (3.3), we get

$$
L_{I_r^{\Phi_B}}(s) = \mathbb{E}_{I_r^{\Phi_B}}[e^{-sI_r^{\Phi_B}}] = \mathbb{E}_{\{h_\mathbf{x}\},\Phi_B}\left[\exp\left(-s\sum_{\mathbf{x}\in\Phi_B/b_0} P_B h_\mathbf{x}\|\mathbf{x}\|^{-\alpha}\right)\right]
$$

$$
\overset{(a)}{=} \mathbb{E}_{\{h\},\Phi_B}\left[\prod_{\mathbf{x}\in\Phi_B/b_0}[\exp(-sP_B h\|\mathbf{x}\|^{-\alpha})]\right]
$$

$$
\overset{(b)}{=} \mathbb{E}_h \exp\left(-2\pi\lambda\int_r^\infty [1 - \exp(-sP_B ht^{-\alpha})]tdt\right) \tag{3.8}
$$

$$
\overset{(c)}{=} \mathbb{E}_h \exp\left(-\pi\lambda(sP_B h)^{\frac{2}{\alpha}}\int_{sP_B hr^{-\alpha}}^0 [1 - \exp(-z)]dz^{-\frac{2}{\alpha}}\right).
$$

Equality (a) is due to i.i.d. random variables $\{h_\mathbf{x} : \mathbf{x} \in \Phi_B/b_0\}$, equality (b) is derived by uti-

lizing probability generating functional(PGFL) of Poisson point process [Stoyan et al. (1995)], and conducting the resolution from cartesian to polar coordination. Note that the integration starts at $t = r$, not the origin, because all the active base stations contributing to $I_r^{\Phi_B}$ lies in the region $\{\mathbf{x} \in \mathbb{R}^2 : \|\mathbf{x}\| \geq r\}$, and equality (c) is due to $z = -sP_Bht^{-\alpha}$. Let $S = sP_Bhr^{-\alpha}$, and consider the integration of (a) in E.q. (3.8).

$$
\int_S^0 [1 - \exp(-z)]dz^{-\frac{2}{\alpha}} = \int_0^S [\exp(-z) - 1]dz^{-\frac{2}{\alpha}}
$$

$$
= \left([\exp(-z) - 1]z^{-\frac{2}{\alpha}}\Big|_0^S + \int_0^S z^{-\frac{2}{\alpha}}\exp(-z)dz \right)
$$

$$
= [\exp(-S) - 1]S^{-\frac{2}{\alpha}} + (\Gamma(1 - \frac{2}{\alpha}) - \Gamma(1 - \frac{2}{\alpha}, S)).
$$

(3.9)

Substitute E.q. (3.9) into E.q. (3.8) and let $s = \frac{Tr^\alpha}{P_B}$ and $\delta = \frac{2}{\alpha}$. Hence,

$$
L_{I_r^{\Phi_B}}(s)\big|_{s=\frac{Tr^\alpha}{P_B}} = \exp\left(-\pi\lambda r^2[-1 + \rho(T, \delta)]\right),
$$

(3.10)

where $\rho(T, \delta) = \frac{1}{1+T} + \mathbb{E}_h[(Th)^\delta(\Gamma(1 - \delta) - \Gamma(1 - \delta, Th)]$.

Hence, the coverage probability of typical downlink is

$$
\mathbb{P}_c^{HD} = \mathbb{E}_r[\mathbb{P}[SINR_D^H > T|r]]
$$

$$
= \int_0^\infty \exp\left(-\frac{Tr^\alpha N_0}{P_B} - \lambda\pi r^2[-1 + \rho(T, \delta)]\right)f_r(r)dr
$$

$$
= \int_0^\infty 2\pi\lambda r \exp\left(-\frac{Tr^\alpha N_0}{P_B} - \lambda\pi r^2\rho(T, \delta)\right)dr.
$$

(3.11)

□

If background noise is neglected (i.e. $N_0 = 0$), then the coverage probability of typical downlink is derived in closed-form: $\mathbb{P}_c^{HD} = \frac{1}{\rho(T,\delta)}$.

As for uplink transmission in half duplex cellular networks, the typical receiving base station b_0 is assumed to locate at the origin of the plane, while the typical transmitting mobile user is denoted as u_0. Similar to downlink transmission, u_0 is the nearest mobile user to the base station b_0. Then, the uplink typical link's $SINR_U^H$ is expressed as

$$SINR_U^H = \frac{P_U h_0 r^{-\alpha}}{N_0 + I_r^{\Phi_U}}, \tag{3.12}$$

where $r = \|u_0\|$ is the link distance, h_0 is the power of rayleigh fading channel between b_0 and u_0, and $I_r^{\Phi_U}$ is the aggregate interference from concurrent downlink transmissions of mobile users stations, described as

$$I_r^{\Phi_U} = \sum_{\mathbf{x} \in \Phi_U / u_0} P_U h_{\mathbf{x}} \|\mathbf{x}\|^{-\alpha}. \tag{3.13}$$

After similar derivation with downlink coverage, the uplink coverage probability is presented in following theorem.

Theorem 3.2. *The uplink coverage probability of the typical link in half duplex cellular network is*

$$\mathbb{P}_c^{HU} = \int_0^\infty 2\pi\lambda r \exp\left(-\frac{Tr^\alpha N_0}{P_U} - \lambda\pi r^2 \rho(T, \delta)\right) dr \tag{3.14}$$

where $\rho(T, \delta) = \frac{1}{1+T} + \mathbb{E}_h[(Th)^\delta(\Gamma(1 - \delta) - \Gamma(1 - \delta, Th)]$ with h following unit exponential distribution.

Consider the analytical results of Theorem 3.1 and Theorem 3.2. When noise is neglected, the coverage probability of typical uplink and downlink are independent of network density, and the coverage probability of typical uplink and downlink are equal. When the noise needs to considered, the signal to noise ratio (SNR) affects the coverage probability. If SNR is decreased, then the coverage probability decreases for both typical uplink and downlink, which is corresponding to the practical results.

3.4 Coverage Probability in the Full Duplex Cellular Network

In this section, we analyze the coverage probability of downlink and uplink in full duplex cellular networks. Base stations are equipped with full duplex radios, making it reality to run uplink and downlink transmission simultaneously on the same frequency. For a typical uplink or downlink transmission, the aggregate interference is from both base stations and uplink transmitting mobile users. To capture the aggregate interference, a two-layer Poisson point process is modeled as the full duplex cellular network, with Poisson point process Φ_B for base stations and Poisson point process Φ_U for uplink mobile users with the same density λ.

Considering a typical uplink transmission, assume that receiving base station b_0 of the typical link is located at the origin. The typical link SINR_U^F is expressed as

$$SINR_U^F = \frac{P_U h_0 r^{-\alpha}}{N_0 + I_{up} + I_{down}}, \tag{3.15}$$

where $r = \|u_0\|$ is the link distance, I_{up} is total interference received from all uplink mobile users except u_0, and I_{down} is the total interference received from all downlink base stations Φ_B. The downlink interference I_{up} and uplink interference I_{up} are formulated as

$$\begin{cases} I_{up} = \sum\limits_{\mathbf{x} \in \Phi_U / u_0} P_u h_{\mathbf{x}} \|\mathbf{x}\|^{-\alpha}, \\ I_{down} = \sum\limits_{\mathbf{x} \in \Phi_B / b_0} P_B h_{\mathbf{x}} \|\mathbf{x}\|^{-\alpha}. \end{cases} \tag{3.16}$$

Then, the uplink coverage probability $\mathbb{P}_c^{FU}$ is expressed as

$$
\begin{aligned}
\mathbb{P}_c^{FU} &= \mathbb{E}_r[\mathbb{P}[SINR_U^F > T|r]] \\
&= \int_0^\infty \mathbb{P}[SINR_D^H > T|r]f_r(r)dr \\
&= \int_0^\infty \mathbb{P}[h_0 > \frac{Tr^\alpha(N_0 + I_{up} + I_{down})}{P_U}]f_r(r)dr \\
&= \int_0^\infty [\exp(-sN_0)L_{I_{up}}(s)L_{I_{down}}(s)]|_{s=\frac{Tr^\alpha}{P_U}} f_r(r)dr.
\end{aligned}
\tag{3.17}
$$

Refering to Theorem 3.2, we can get

$$
L_{I_{up}}(s)|_{s=\frac{Tr^\alpha}{P_U}} = \exp\left[\lambda\pi r^2 \left(1 + \rho(T,\delta)\right)\right].
\tag{3.18}
$$

According to Palm theory [Stoyan et al. (1995)], all the base stations but b_0 that contribute to I_{down} also follows Poisson point process when viewed from typical node b_0. Thus,

$$
\begin{aligned}
L_{I_{down}}(s)|_{s=\frac{Tr^\alpha}{P_U}} &= \mathbb{E}_h \exp\left(-2\pi\lambda \int_0^\infty [1 - \exp\left(-\frac{P_B Tr^\alpha ht^{-\alpha}}{P_U}\right)]tdt\right) \\
&\overset{(a)}{=} \mathbb{E}_h \exp\left(-\frac{2\pi\lambda}{\alpha} \int_0^\infty [1 - \exp\left(-\frac{P_B Tr^\alpha hy}{P_U}\right)]y^{-\frac{2}{\alpha}-1}dy\right) \\
&\overset{(b)}{=} \exp\left(-\frac{\pi\lambda r^2 P_B T^\delta}{P_U}\mathbb{E}_h[h^\delta]\Gamma(1-\delta)\right) \\
&\overset{(c)}{=} \exp\left(-\frac{\pi\lambda r^2 P_B T^\delta}{P_U}\Gamma(1+\delta)\Gamma(1-\delta)\right) \\
&= \exp\left(-\frac{\pi\lambda r^2 P_B T^\delta}{P_U}\cdot\frac{\pi\delta}{\sin(\pi\delta)}\right).
\end{aligned}
\tag{3.19}
$$

Note that equality (a) follows that $y = t^{-\alpha}$, equality (b) follows that $z = \frac{P_B Tr^\alpha hy}{P_U}$ and the definition of Gamma function, and equality (c) is due to Rayleigh fading channel.

Substitute E.q. (3.18) and E.q. (3.19) into E.q. (3.17), we get follow theorem:

Theorem 3.3. *The typical uplink coverage probability in the full duplex cellular network is*

$$\mathbb{P}_c^{FU} = \int\limits_{r>0} 2\pi\lambda r \exp\left(-\frac{Tr^\alpha N_0}{P_U} - \lambda\pi r^2[\rho(T,\delta) + \varphi(\frac{TP_B}{P_U},\delta)]\right)dr, \qquad (3.20)$$

where $\varphi(\frac{TP_B}{P_U},\delta) = \frac{P_B T^\delta}{P_U} \cdot \frac{\pi\delta}{\sin(\pi\delta)}$, and $\rho(T,\delta) = \frac{1}{1+T} + \mathbb{E}_h[(Th)^\delta(\Gamma(1-\delta) - \Gamma(1-\delta,Th)]$ with h following unit exponential distribution.

As for downlink transmission, the typical receiving base station b_0 is located at the origin. The link $SINR_D^F$ can be expressed as

$$SINR_D^F = \frac{P_B h_0 r^{-\alpha}}{N_0 + I'_{up} + I'_{down}}, \qquad (3.21)$$

where I'_{up} is total interference received from all uplink mobile users except u_0, and I'_{down} is the total interference received from all downlink base stations except b_0, expressed as

$$\begin{cases} I_{up} = \sum\limits_{\mathbf{x}\in\Phi_U/u_0} P_u h_{\mathbf{x}}\|\mathbf{x}\|^{-\alpha}, \\ I_{down} = \sum\limits_{\mathbf{x}\in\Phi_B/b_0} P_B h_{\mathbf{x}}\|\mathbf{x}\|^{-\alpha}. \end{cases} \qquad (3.22)$$

Derive the downlink coverage probability similar to uplink transmission. We get following theorem.

Theorem 3.4. *The typical downlink coverage probability in the full duplex cellular network is*

$$\mathbb{P}_c^{DF} = \int\limits_{r>0} 2\pi\lambda r \exp\left(-\frac{Tr^\alpha N_0}{P_B} - \lambda\pi r^2[\rho(T,\delta) + \varphi(\frac{TP_U}{P_B},\delta)]\right)dr, \qquad (3.23)$$

where $\varphi(\frac{TP_U}{P_B},\delta) = \frac{P_U T^\delta}{P_B} \cdot \frac{\pi\delta}{\sin(\pi\delta)}$, and $\rho(T,\delta) = \frac{1}{1+T} + \mathbb{E}_h[(Th)^\delta(\Gamma(1-\delta) - \Gamma(1-\delta,Th)]$ with h following unit exponential distribution.

It can be concluded that the transmission power ratio between base stations and mobile terminals affects the coverage probability of both typical uplink and downlink in full duplex cellular network, and the coverage probability is independent with network density when noise is neglected.

3.5   Mutual Interference Cancelation at Base Stations

Full duplex communications create more opportunities for transmissions and/or receptions in wireless networks, but the severe aggregation limits the network capacity improvements. Here, mutual interference cancelation is put forward and analyzed. Due to the power functionality of base stations, assume that base stations can realize mutual interference cancelations via exchanging information signals through smart antennas or optical fiber.

Mutual interference cancelation at a base station only empowers the base station to cancel the interference from current active base stations' uplink transmissions, hence, only improves the uplink data transmission. We assume perfect cancelation where the aggregate interference from all base stations are canceled completely, and present the improvement on the typical uplink transmission.

Perfect mutual interference cancelation on the base stations makes typical uplink transmission escape interference from active base stations' uplink transmissions in the full duplex cellular networks, i.e. $I_{down} = 0$ in E.q (3.22). Thus, the SINR of the typical uplink after perfect mutual interference cancelation in full duplex cellular network is equal to the SINR of the typical uplink in half duplex cellular network. Thus, it is concluded that perfect mutual interference cancelation improves the uplink coverage probability equal to that in half duplex cellular network, i.e. $P_c^{MUF} = P_c^{UH}$.

3.6 Numerical Results and Discussions

In this section, numerical results are presented on coverage probability and average rate of a typical link in a large scale full duplex cellular network, and comparison with half duplex communication is conducted to depict the network capacity gain of full duplex communication. Two scenarios are considered, zero background noise scenario and nonzero background noise scenario. The path loss model is set as $g(\mathbf{x}) = \frac{1}{\|\mathbf{x}\|^\alpha}$ with $\alpha = 4$. Then, $\delta = \frac{1}{2}$ and the common used parameter $\rho(T, \delta)$ can be derived into following closed-form,

$$\rho(T, \delta) = 1 + \sqrt{T}(\pi/2 - \arctan(1/\sqrt{T})),$$

which can be obtained by deriving E.q. (3.8) with first variable expectation calculations of h, and Φ later.

3.6.1 Zero Background Noise Scenario

When the background noise is zero, we can get the coverage probability of typical uplink and downlink in half duplex and half duplex cellular networks.

$$\begin{cases} \mathbb{P}_c^{UH}(T) = \frac{1}{\rho(T,\delta)} = \frac{1}{1+\sqrt{T}(\pi/2-\arctan(1/\sqrt{T}))}; \\ \mathbb{P}_c^{DH}(T) = \frac{1}{\rho(T,\delta)} = \frac{1}{1+\sqrt{T}(\pi/2-\arctan(1/\sqrt{T}))}; \\ \mathbb{P}_c^{UF}(T) = \frac{1}{\rho(T,\delta)+\varphi(\frac{TP_B}{P_U},\delta)} = \frac{1}{1+\sqrt{T}(\pi/2-\arctan(1/\sqrt{T}))+\frac{\pi P_B}{2P_U}\sqrt{T}}; \\ \mathbb{P}_c^{DF}(T) = \frac{1}{\rho(T,\delta)+\varphi(\frac{TP_U}{P_B},\delta)} = \frac{1}{1+\sqrt{T}(\pi/2-\arctan(1/\sqrt{T}))+\frac{\pi P_U}{2P_B}\sqrt{T}}. \end{cases} \quad (3.24)$$

It can be easily obtained that the coverage probability and average rate is independent of network density in zero background noise scenario.

Coverage probability of typical uplink and downlink is showed in Fig. 3.4 with three down-up-link transmission power ratio $\frac{P_B}{P_U} = 1, 4, 0.25$. Conclusions are drew as follows. Firstly,
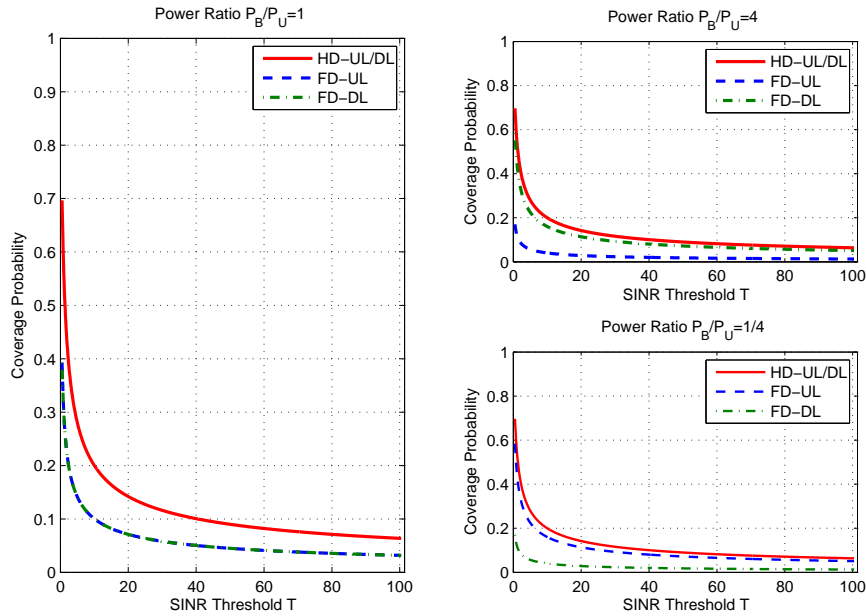
Figure 3.4: Coverage probability of typical uplink and downlink in half duplex and full duplex cellular networks with zero background noise.

Coverage probability of typical uplink and downlink are equal with each other in half duplex cellular network, and coverage probability of typical link in half duplex is always larger than that in full duplex for both uplink and downlink. Secondly, in full duplex cellular network, coverage probability of typical uplink is larger than coverage probability of typical downlink if down-up-link transmission power ratio $\frac{P_B}{P_U}$ less than 1, larger if down-up-link transmission power ratio $\frac{P_B}{P_U}$, and equal when down-up-link transmission power ratio $\frac{P_B}{P_U} = 1$. Thirdly, if down-up-link transmission power ratio $\frac{P_B}{P_U}$ approaches 0, coverage probability of full duplex uplink approaches that of half duplex uplink, and if if down-up-link transmission power ratio $\frac{P_B}{P_U}$ approaches ∞, coverage probability of full duplex downlink approaches that of half duplex downlink. The reason is that full duplex uplink becomes the dominant transmission if $\frac{P_B}{P_U}$ approaches 0, while otherwise if $\frac{P_B}{P_U}$ approaches ∞.

Average rate of typical uplink and downlink is showed in Fig. 3.5 that corresponding to setting in Fig. 3.4. Legend HD and FD represents half duplex and full duplex cellular network, UL and DL represents typical uplink and downlink. HD-UL/DL represents average rate of
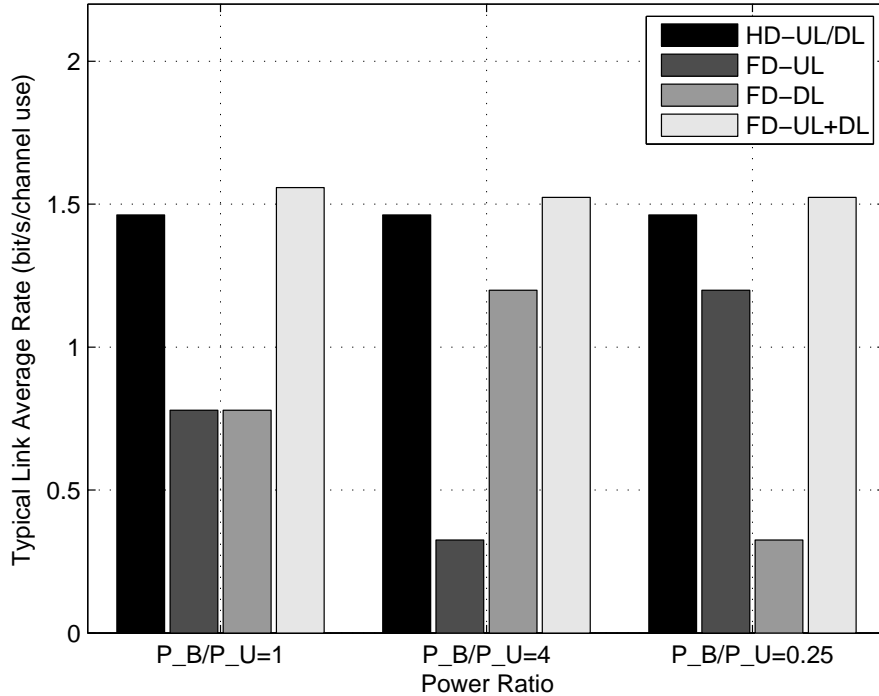
Figure 3.5: Average rate of typical uplink and downlink in half duplex and full duplex cellular networks with zero background noise.

typical uplink or downlink in half duplex cellular network, and FD-UL+DL represents sum average rate of typical uplink and downlink in half duplex cellular network. We can conclude following statements from Fig. 3.5. Firstly, average rate of typical uplink and downlink in half duplex cellular network are always larger than those in full duplex cellular network. Secondly, for both full duplex and half duplex cellular networks, average rate of typical downlink is larger than that of uplink if down-up-link transmission power ratio $\frac{P_B}{P_U}$ is larger than 1, and otherwise if down-up-link transmission power ratio $\frac{P_B}{P_U}$ is less than 1. Thirdly, sum average rate of uplink and downlink in full duplex cellular network is always larger than that of uplink or downlink in half duplex cellular network, but the difference is not so large.

Network capacity gain of full duplex communication, defined by the cell average rate ratio between full duplex and half duplex cellular networks, is presented in Fig. 3.6 for different down-up-link transmission power ratio $\frac{P_B}{P_U}$, where average cell rate is the sum average rate of uplink
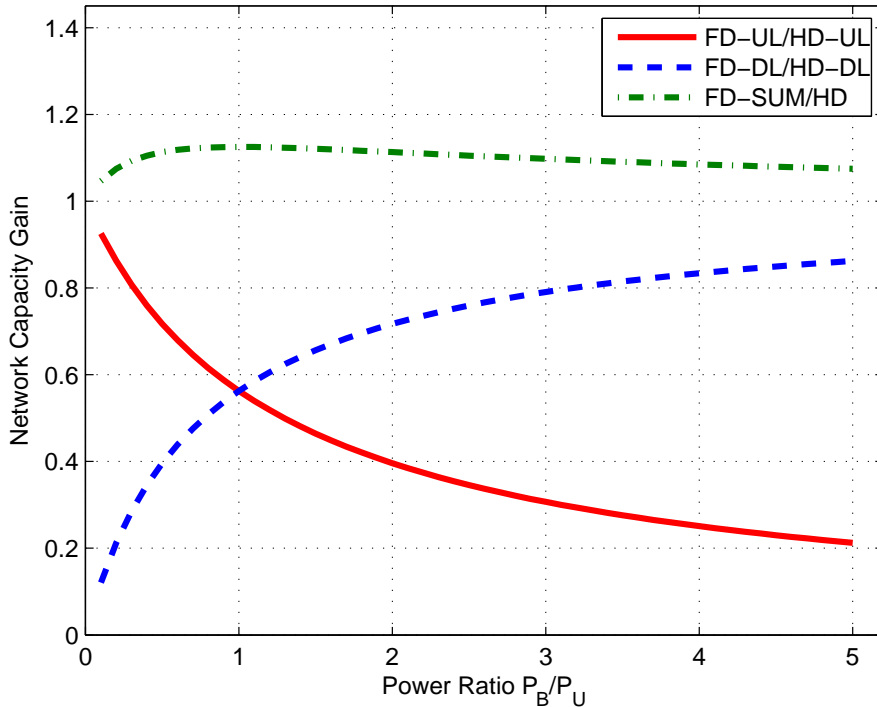
Figure 3.6: Network capacity gain of full duplex communication in cellular networks with zero background noise.

and downlink in a cell. Due to equality of uplink and downlink in half duplex cellular network, network capacity gain doesn't change alternatively. Firstly, network capacity gain of full duplex communication, represented by the dotted dash line, just lies in $(1, 1.2)$, thus it is very limited. Moreover, the network capacity gain get the maximum value when $\frac{P_B}{P_U} = 1$. Secondly, the rate ratio of uplink between full duplex communication and half duplex communication decreases from 1 to 0.2 and the rate ratio of downlink between full duplex communication and half duplex communication increases from 0 to 0.9 when $\frac{P_B}{P_U}$ increase from 0.1 to 5.1. The key reason is that downlink transmission is dominant when $\frac{P_B}{P_U}$ is large.

In Fig. 3.7, the network capacity gain of full duplex communication in cellular network with/without mutual interference cancelation is depicted. It can be concluded that mutual interference cancelation improve the network capacity gain significantly and the improvement becomes larger as $\frac{P_B}{P_U}$ increase from 0.1 to 5.1. The reason is that perfect mutual interfer-
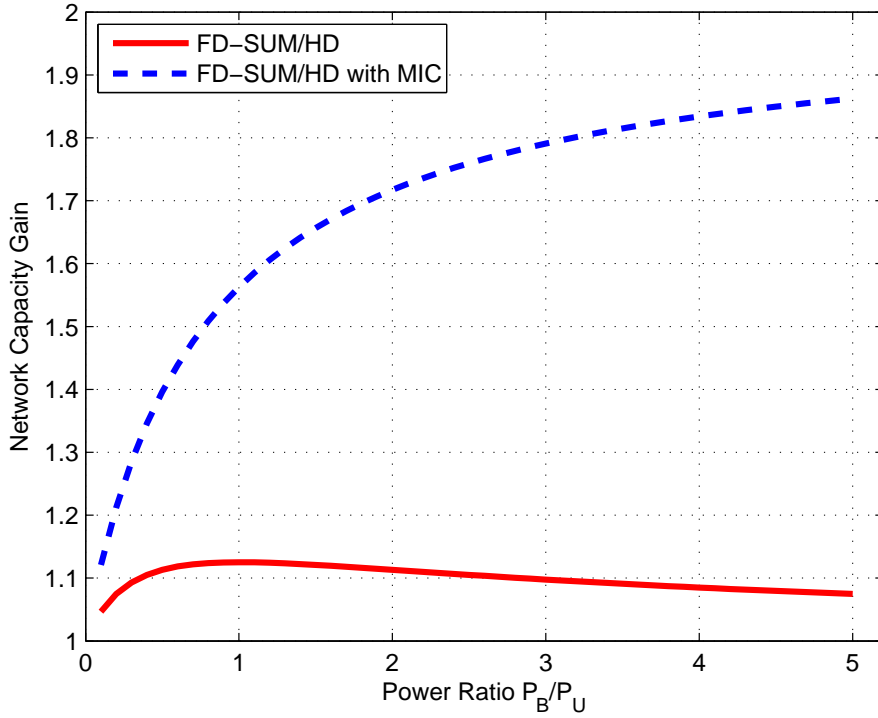
Figure 3.7: Network capacity gain of full duplex communication in cellular network with/without mutual interference cancelation of zero background noise.

ence cancelation is assumed to conduct between full duplex downlink transmission pairs, and downlink transmission dominates when $\frac{P_B}{P_U}$ is large.

3.6.2 Nonzero Background Noise Scenario

As for nonzero background noise scenario, coverage probability can be derived to a closed-from result when $\alpha = 4$, since

$$
\begin{aligned}
\int_0^\infty \exp(-ax)\exp(-bx^2)dx &= \int_0^\infty \exp(-(\sqrt{b}x + \frac{a}{2\sqrt{b}})^2 + \frac{a^2}{4b})dx \\
&= \exp(\frac{a^2}{4b})\int_0^\infty \exp(-(\sqrt{b}x + \frac{a}{2\sqrt{b}})^2)dx \\
&= \sqrt{\frac{\pi}{b}}\exp(\frac{a^2}{4b})Q(\frac{a}{\sqrt{2b}}),
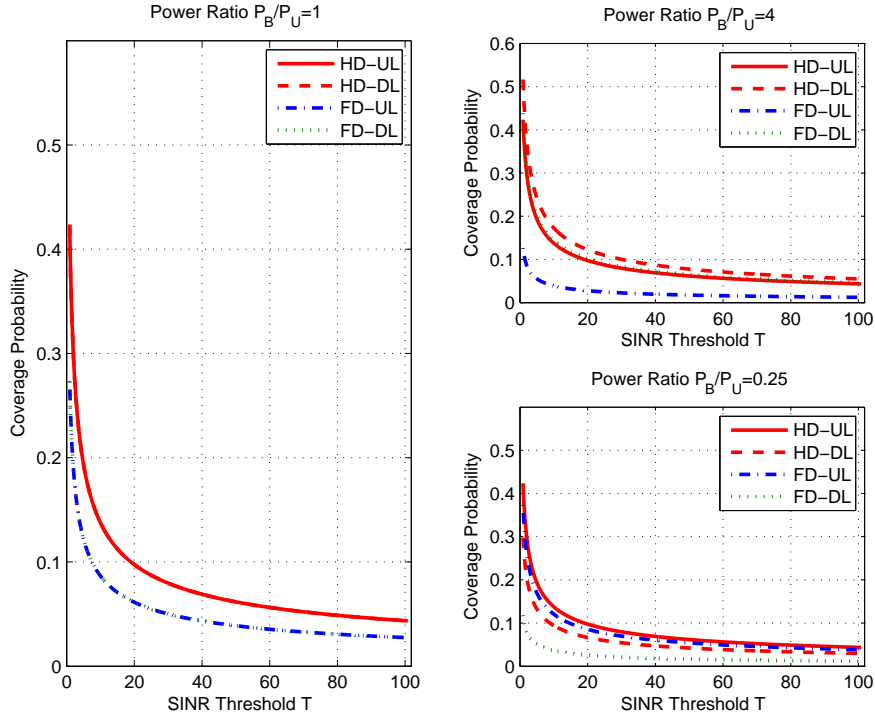\end{aligned}
$$

Figure 3.8: Coverage probability of typical uplink and downlink in half duplex and full duplex cellular networks with nonzero background noise. $SNR = 10dB$ and network density is 0.1.

where $Q(x) = \frac{1}{\sqrt{2\pi}} \int_x^\infty \exp(-\frac{y^2}{2})$. Let $K_D = \frac{N_0 T}{P_B}$, $K_U = \frac{N_0 T}{P_U}$, $C_H = \pi\lambda\rho(T,\delta)$, $C_F^U = \pi\lambda[\rho(T,\delta) + \varphi(\frac{TP_B}{P_U},\delta)]$ and $C_F^D = \pi\lambda[\rho(T,\delta) + \varphi(\frac{TP_U}{P_B},\delta)]$. The coverage probability of typical uplink and downlink in full duplex and half duplex cellular networks are expressed as

$$
\begin{cases}
\mathbb{P}_c^{UH}(T) = \int_0^\infty \pi\lambda e^{-K_U v^2} e^{-C_H v} dv = \sqrt{\frac{\pi}{K_U}} \exp(\frac{C_H{}^2}{4K_U}) Q(\frac{C_H}{\sqrt{2K_U}}); \\
\mathbb{P}_c^{DH}(T) = \int_0^\infty e^{-K_D v^2} e^{-C_H v} dv = \sqrt{\frac{\pi}{K_D}} \exp(\frac{C_H{}^2}{4K_D}) Q(\frac{C_H}{\sqrt{2K_D}}); \\
\mathbb{P}_c^{UF}(T) = \int_0^\infty e^{-K_U v^2} e^{-C_F^U v} dv = \sqrt{\frac{\pi}{K_U}} \exp(\frac{C_F^U{}^2}{4K_U}) Q(\frac{C_F^U}{\sqrt{2K_U}}) \\
\mathbb{P}_c^{DF}(T) = \int_0^\infty e^{-K_D v^2} e^{-C_F^D v} dv = \sqrt{\frac{\pi}{K_D}} \exp(\frac{C_F^D{}^2}{4K_D}) Q(\frac{C_F^D}{\sqrt{2K_D}}).
\end{cases}
\tag{3.25}
$$

Thus, under the communication scenario with background noise, the coverage probability is related to network density in both half duplex and full duplex cellular networks. Denote $SNR = 10\log 10(P_U/N_0)$ as the signal to noise ratio of mobile users in the cellular networks.

Coverage probability of typical uplink and downlink is showed in Fig. 3.8 with three down-

up-link transmission power ratio $\frac{P_B}{P_U} = 1, 4, 0.25$. Similar to zero noise scenario, coverage probability of typical link in half duplex is always larger than that in full duplex for both uplink and downlink. But coverage probability of typical uplink is larger than coverage probability of typical downlink if down-up-link transmission power ratio $\frac{P_B}{P_U}$ less than 1, larger if down-up-link transmission power ratio $\frac{P_B}{P_U}$, and equal when down-up-link transmission power ratio $\frac{P_B}{P_U} = 1$ in both half duplex and full duplex cellular network. Moreover, coverage probability of typical downlink in full duplex communication is larger than that of typical uplink in half duplex communication when down-up-link transmission power ratio $\frac{P_B}{P_U} = 4$, and coverage probability of typical uplink in full duplex communication is larger than that of typical downlink in half duplex communication when down-up-link transmission power ratio $\frac{P_B}{P_U} = 0.25$. It indicates that network capacity gain of full duplex communication is relatively large when compared with uplink transmission of half duplex communication in high down-up-link transmission power ratio region and downlink transmission of half duplex communication in low down-up-link transmission power ratio region.

Based on Fig. 3.8, average rate of typical uplink and downlink is showed in Fig. 3.9. Legend HD and FD represents half duplex and full duplex cellular network, UL and DL represents typical uplink and downlink. FD-UL+DL represents sum average rate of typical uplink and downlink in half duplex cellular network. Firstly, average rate of typical uplink and downlink in half duplex cellular network are always larger than those in full duplex cellular network for all down-up-link transmission power ratio $\frac{P_B}{P_U}$, but the average cell rate of full duplex communication is always larger than that of uplink or downlink in half duplex cellular network, and the average uplink rate of full duplex communication is much less than that of half duplex communication when $\frac{P_B}{P_U} = 4$, indicating aggregate interference was very severe for uplink in full duplex communication. Similar results happen to average downlink when $\frac{P_B}{P_U} = 0.25$.

In Fig. 3.10, the network capacity gain of full duplex communication in cellular network with/without mutual interference cancelation is depicted. From the left sub-figure, it can be
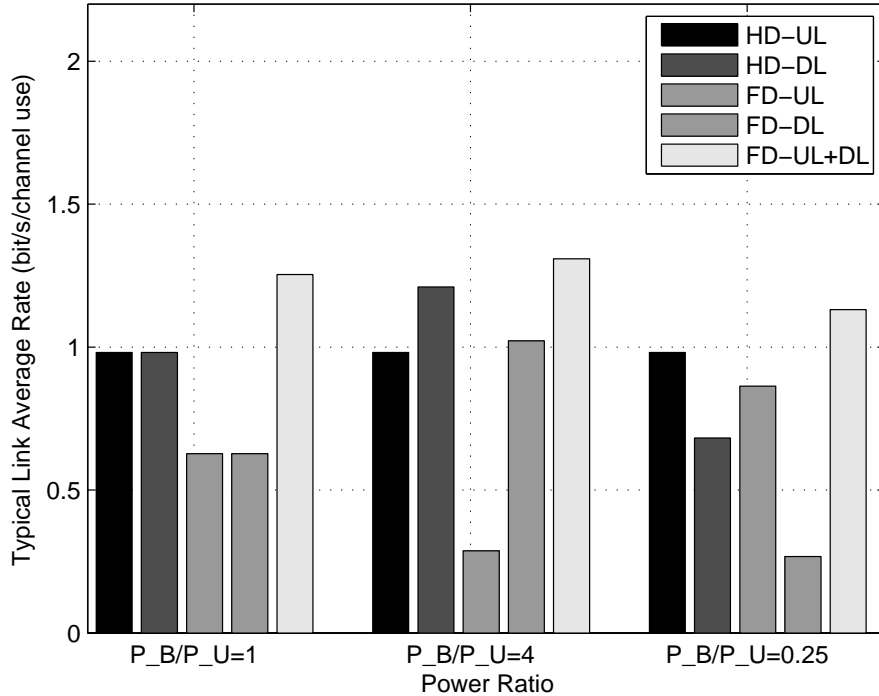
Figure 3.9: Average rate of typical uplink and downlink in half duplex and full duplex cellular networks with zero background noise. $SNR = 10dB$ and network density is 0.1.

concluded that as down-up-link transmission power ratio increases, the average uplink ratio between full duplex and half duplex cellular networks decreases from 1.0 to 0.2, while average downlink ratio between full duplex and half duplex cellular networks decreases from 0.2 to 0.9. The key reason is that high down-up-link transmission power ratio introduce severe aggregate interference on uplink transmission. Thus, the ratio between mean cell rate of full duplex cellular network and uplink transmission in half duplex cellular network decreases, showed from 2.2 to 1.1. In the same time, the ratio between mean cell rate of full duplex cellular network and downlink transmission in half duplex cellular network increases, showed from 1.1 to 1.4. Thus, depicted in right sub-figure, the mean network capacity gain of full duplex communication is very limited, and decreases from 1.45 to 1.18, while Mutual interference cancelation improve the network capacity gain significantly and the network capacity gain increase from 1.5 to 1.9.

In Fig. 3.11 network capacity gain of dull duplex communication is exploited in cellular
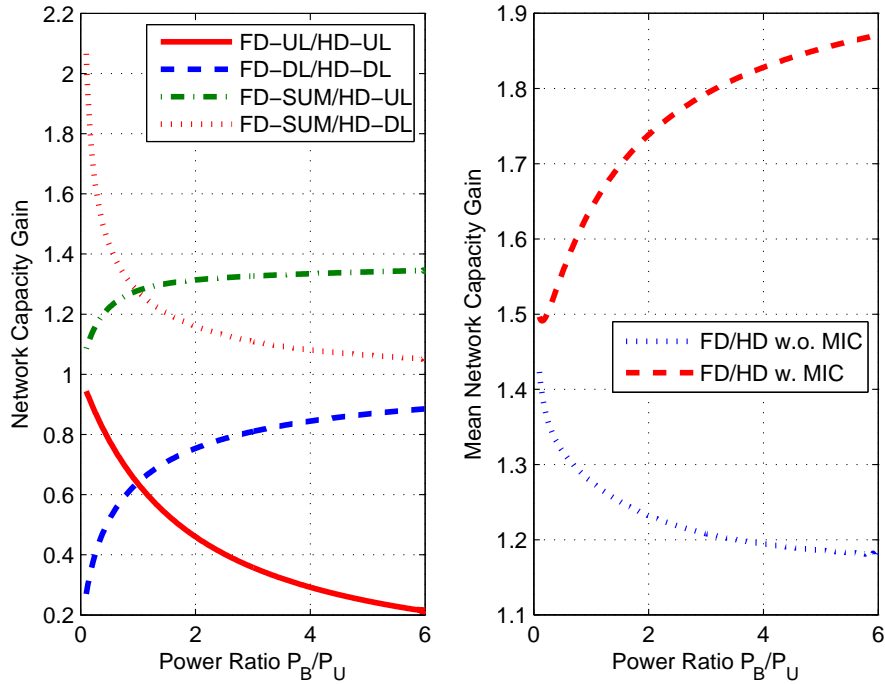
Figure 3.10: Network capacity gain of full duplex communication in cellular network with/without mutual interference cancelation of nonzero background noise.

network under different uplink SNR value. The network density is 0.1 and $\frac{P_B}{P_U} = 1.5$. Conclusions are made for left sub-figure: network capacity gain of full duplex communication in cellular network decreases as SNR increases; The ratio of uplink transmission, and the ratio of downlink transmission between full duplex and half duplex cellular networks, decreases as SNR increases; As for average cell rate, the ratio between full duplex communication and uplink or downlink transmission decreases as SNR increases. For the right sub-figure, we can conclude that mutual interference improves the network capacity gain significantly, but can't change the trend with SNR.

Fig. 3.12 presents the relationship between network density and network capacity gain of full duplex cellular network with $SNR = 10dB$ and down-up-link transmission power ratio $\frac{P_B}{P_U} = 2$. Firstly, the network capacity defined by network density times average rate is drew in the left figure, and the network density increase almost linearly with network density. For both right figures, it can be seen that network capacity gain from full duplex communication
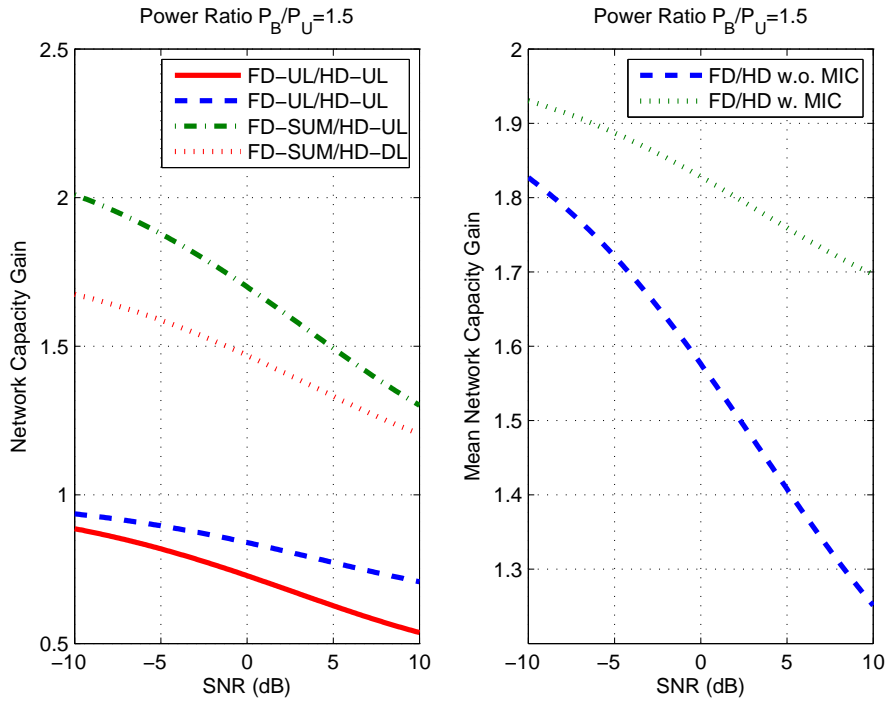
Figure 3.11: Network capacity gain of full duplex communication in cellular network with/without mutual interference cancelation of nonzero background noise under different SNR.

decreases as network density increases. Moreover, the ratio of uplink transmission, and the ratio of downlink transmission between full duplex and half duplex cellular networks, decreases as network density increases. So do the ratio of average cell rate between full duplex cellular network and uplink or downlink transmission in half duplex cellular network. But the change is relatively insignificant. From the bottom of the right figure, mutual interference cancelation's improvement is become more significant as network density increases. Thus, high transmission density for cellular network reduce network capacity gain of full duplex communication. The reason is that large network density introduces severe aggregate interference as the bottleneck for network capacity.
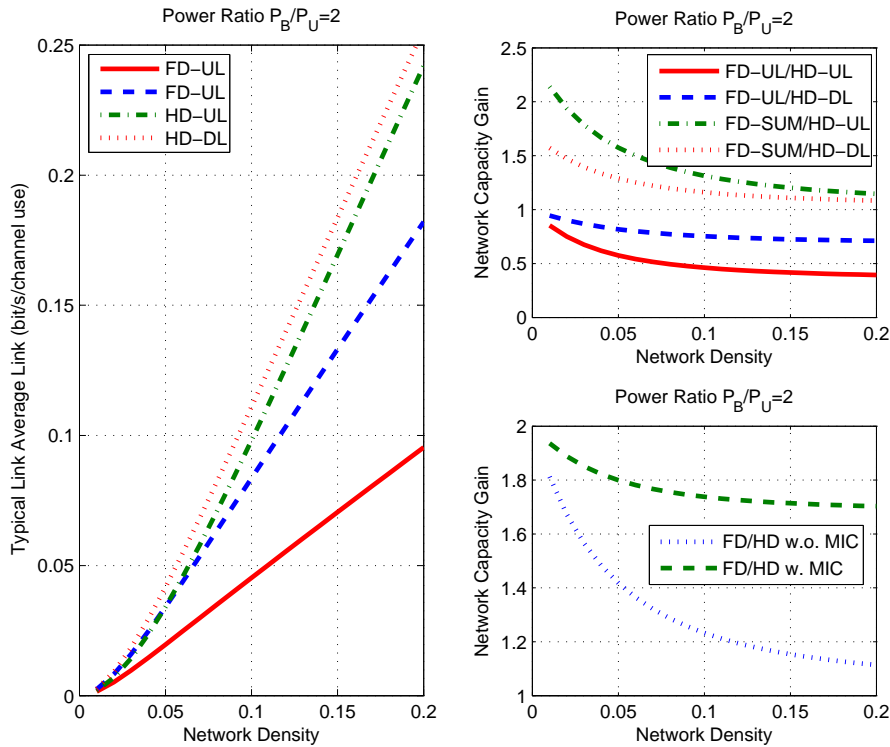
Figure 3.12: Network capacity gain of full duplex communication in cellular network with/without mutual interference cancelation of nonzero background noise under different Network Density .

3.7 Summary

In this chapter, network capacity gain of full duplex communications is analyzed in a large scale cellular network, and mutual interference cancelation technique is put forward to combat severe aggregate interference. Two-layer Poisson point process is designed for the network topology, and the coverage probability and average rate of typical uplink and downlink are derived. Numerical simulations are presented for niose and noise-free communication scenarios. For noise-free cellular networks, the average rate and coverage probability of typical uplink and downlink are expressed in closed-form and proved to be correlated with transmission power ratio between base stations and mobile users, while independent of network density. As for full duplex cellular networks with background noise, derivation of some special case ($\alpha = 4$) is

presented in closed-from based on norm distribution function. Our analytical and numerical results reveal the limitations of full duplex communications in cellular networks and the effective improvement of perfect mutual interference cancelation technique. Thus, it is confirmed that severe aggregate interference limits the network capacity gain of full duplex communications in a large scale cellular network. More practical details on mutual interference technique are left for future research.

Chapter 4

Conclusion

Full duplex communication introduces a new degree of freedom for theoretical analysis in wireless networks. In this thesis, network capacity gain of two types of full duplex wireless networks were studied via stochastic geometry, including ad hoc wireless network and cellular wireless network. We first investigated the transmission capacity of a full duplex wireless ad hoc network with BDF mode, defined as the maximum throughput in an unit area, subjecting to a fixed link rate and a constraint of outage probability. Network topology were modeled by Thomas cluster point process and we proposed new Palm theory, cluster Palm theory, to assist the description for the aggregate interference of a typical link. Analytical results on two generalized transmission capacity definitions, maximum transmission throughput via maximizing network density for fixed link rate and maximum transmission throughput via maximizing link rate for fixed network density, were derived for both half duplex and full duplex ad hoc networks. Our numerical results show that network capacity gain of full duplex communication over half duplex communication is very limited and provide insights for system conditions to utilize full duplex communication's advantage completely.

In the second topic, average rate and coverage probability of typical uplink and downlink were studied in a full duplex cellular network with FDR mode. Two-layer Poisson point process

was adopted to be the network topology. The aggregate interference on the typical link was derived carefully with the consideration for unique deployment of base stations and mobile users in cellular network. Mutual interference cancelation technique was put forward and assumed to conduct between uplink pairs via functionality of base stations. Analytical derivation of average rate and coverage probability for the uplink and downlink were presented in closed-form in noise free half duplex and full duplex cellular networks. For some typical case, the results are in closed-form when considering non-zero noise cellular networks. Numerical results show the limited network capacity gain of full duplex communication in cellular network and the significant improvement of mutual interference cancelation technique.

4.1   Contributions

The following contributions are made in this thesis:

- In Chapter 2, Thomas cluster point process was leveraged to model the network topology of a large scale full duplex cellular network. Tail probability function of aggregate interference of typical link were derived, and compared with half duplex ad hoc network, analytical results shows that full duplex communications make the interference distribution more dispersed. Two generalized types of transmission capacity of full duplex wireless ad hoc network were derived. We found that in high density networks, full duplex network capacity gain over half duplex communication is very low, less than 0.6, which is far from expected gain 2.0, while in low density networks, the network gain approaches expected gain 2.0, but the network lack spatial reuse. Moreover, we also found that network capacity gain of full duplex communications always larger than 1.0, and increases as link rate increase. But the maximum gain in our numerical results is just 1.35, which is far less than expected. Thus, our analytical and numerical results show the limitation of network capacity gain of full duplex communication in wireless ad hoc network. To

our best knowledge, this is the first paper to analyze full duplex network capacity gain in large scale ad hoc network via stochastic geometry. Research work from this topic results in a paper (Wang and Huang, 2014).

- In Chapter 3, two-layer Poisson point process was designed for the network topology for a large scale full duplex cellular network, and mutual interference cancelation technique was put forward to combat severe aggregate interference. Coverage probability and average rate of typical uplink and downlink in a full duplex cellular network were derived. Based on closed-form derivation, precise numerical results were run for two scenarios, zero and nonzero background noise. For the zero noise cellular networks, we found that network density doesn't affect the coverage probability and average rate in both half duplex and full duplex cellular networks. But for the nonzero noise cellular networks, network density is a factor, and network capacity gain of full duplex communication decreases as network density increases. Moreover, down-up-link transmission power ratio was investigated and we found that severe aggregate interference impairs uplink transmission in high down-up-link transmission power ratio region and downlink transmission in low down-up-link transmission power ratio region. With fixed down-up-link transmission power ratio, the effect of uplink's signal to noise ratio (SNR) on network capacity gain of full duplex was studied. Results show that the network capacity gain reduce as SNR increases. Our analytical and numerical results reveal the limitations of full duplex communications in cellular networks and the effective improvement of perfect mutual interference cancelation technique. Thus, it is confirmed that severe aggregate interference limits the network capacity gain of full duplex communications in a large scale cellular network. More practical details on mutual interference technique are left for future research.

4.2 Future Works

Despite the contribution that we have made so far, a lot of challenging problems still remains, which can be topics for future research.

In Chapter 2, we simplify the MAC protocols as slotted ALOHA, while wireless used MAC protocol is CSMA/CA in wireless ad hoc networks. It is big research topic to design good MAC protocols under full duplex communication scenarios. Theoretical analysis on how to evaluate the performance of new designed full duplex MAC protocols in large scale wireless networks is very critical research topic. Moreover, another interesting topic is the analysis on network capacity improvement via mutual interference cancelation in full duplex ad hoc network via stochastic geometry.

In Chapter 3, we assume that mobile users are with half duplex radios. It is also important research topic to identify the network capacity gain of full duplex communication when all terminals are installed with full duplex radios in large scale cellular networks. Moreover, practical design of mutual interference cancelation and the joint process with self interference cancelation technique of half duplex communication is still an open problem.

Acknowledgments

I have had a great time at SJTU during my master program. I would not have had such wonderful experience without the help and support from you:

Thank you, Prof. Xudong Wang. It is you who offers me the RA position to graduate study in SJTU and introduces me to the amazing fields of wireless communication and networking. Under your guidance, I have made progress in following aspects, from identifying research topics to finding creative solutions, from writing papers to presenting presentations, and from thinking independently to cooperating with others. Prof. Wang also teaches me how to review papers submitted to top journals and conferences. All these training stimulates my critical thinking and encourages me to get a promising career future.

Thank you, all the group members in Wireless and Networking Lab, including Pengfei Huang, Quan Liu, Pin Lv, Jun Wang, Shanshan Wu, Wenguang Mao, Yibo Pi, Yuhang Zhang, Aiming Tang, Jiawei Chen. It is wonderful experience to work with you in SJTU. It is your accompanies and encourages keep me away from loneliness. We spend lots of time together and enjoy the happiness from sports, research meeting, and parties. The friendships with you are the most valuable treasure in my life.

Thank you, Shuo Huang. As my only roommate, you encourage me a lot when I meet difficulties, and share ideas on life with me. Your humor enrich the time we spend together in our dormitory of R640. I wish you a bright future in your PhD career in the USA. By the way, try to rent a sunthern exposure room. Or, you will continue to experiencing moist summer and

cold winter.

Thank you, mum, dad, brother and girl friend. I would like to express my deepest gratitude to you for the unconditional love, understanding, and encouragement. I love you!

Bibliography

Abramson, N. (1970). The aloha system: another alternative for computer communications. In *Proceedings of the November 17-19, 1970, fall joint computer conference*, pp. 281–285. ACM.

Andrews, J. G., F. Baccelli, and R. K. Ganti (2011). A tractable approach to coverage and rate in cellular networks. *Communications, IEEE Transactions on 59*(11), 3122–3134.

Baccelli, F. and B. Blaszczyszyn (2009). *Stochastic Geometry and Wireless Networks, Part I: Theory*, Volume 1. Now Publishers Inc.

Bharadia, D., E. McMilin, and S. Katti (2013). Full duplex radios. In *Proceedings of the ACM SIGCOMM 2013 conference on SIGCOMM*, pp. 375–386. ACM.

Campbell, N. (1909). The study of discontinuous phenomena. In *Proc. Camb. Phil. Soc*, Volume 15, pp. 310.

Choi, J. I., M. Jain, K. Srinivasan, P. Levis, and S. Katti (2010). Achieving single channel full duplex wireless communication. In *Proceedings of the sixteenth annual international conference on Mobile computing and networking*, MobiCom '10, pp. 1–12. ACM.

Colvin, A. (1983). Csma with collision avoidance. *Computer Communications 6*(5), 227–235.

Esmailzadeh, R. and M. Nakagawa (2003). *TDD-CDMA for wireless communications*. Artech House.

Everett, E., M. Duarte, C. Dick, and A. Sabharwal (2011). Empowering full-duplex wireless communication by exploiting directional diversity. In *Signals, Systems and Computers (ASILOMAR), 2011 Conference Record of the Forty Fifth Asilomar Conference on*, pp. 2002–2006. IEEE.

Ganti, R. K. and M. Haenggi (2009). Interference and outage in clustered wireless ad hoc networks. *IEEE transactions on information theory 55*(9), 4067–4086.

Gollakota, S. and D. Katabi (2008). Zigzag decoding: Combating hidden terminals in wireless networks. In *Proceedings of the ACM SIGCOMM 2008 Conference on Data Communication*, Volume 38, pp. 159–170. ACM.

Gupta, P. and P. R. Kumar (2000). The capacity of wireless networks. *Information Theory, IEEE Transactions on 46*(2), 388–404.

Jain, M., J. I. Choi, T. Kim, D. Bharadia, S. Seth, K. Srinivasan, P. Levis, S. Katti, and P. Sinha (2011). Practical, real-time, full duplex wireless. In *Proceedings of the 17th annual international conference on Mobile computing and networking*, pp. 301–312. ACM.

Ju, H., S. Lim, D. Kim, H. V. Poor, and D. Hong (2012). Full duplexity in beamforming-based multi-hop relay networks. *Selected Areas in Communications, IEEE Journal on 30*(8), 1554–1565.

Kim, S. and W. E. Stark (2013). On the performance of full duplex wireless networks. In *Information Sciences and Systems (CISS), 2013 47th Annual Conference on*, pp. 1–6. IEEE.

Lowen, S. B. and M. C. Teich (1990). Power-law shot noise. *Information Theory, IEEE Transactions on 36*(6), 1302–1318.

Martin, H. (2012). *Stochastic geometry for wireless networks*. Cambridge University Press.

Martin, H., J. G. Andrews, F. Baccelli, O. Dousse, and M. Franceschetti (2009). Stochastic geometry and random graphs for the analysis and design of wireless networks. *Selected Areas in Communications, IEEE Journal on 27*(7), 1029–1046.

Martin, H. and R. K. Ganti (2009). *Interference in large wireless networks*, Volume 3. Now Publishers Inc.

Nguyen, H. Q., F. Baccelli, and D. Kofman (2007). A stochastic geometry analysis of dense ieee 802.11 networks. In *INFOCOM 2007. 26th IEEE International Conference on Computer Communications. IEEE*, pp. 1199–1207. IEEE.

Radunovic, B., D. Gunawardena, P. Key, A. Proutiere, N. Singh, V. Balan, and G. Dejean (2010). Rethinking indoor wireless mesh design: Low power, low frequency, full-duplex. In *Wireless Mesh Networks (WIMESH 2010), 2010 Fifth IEEE Workshop on*, pp. 1–6. IEEE.

Radunovic, B., D. Gunawardena, A. Proutiere, N. Singh, V. Balan, and P. Key (2009). Efficiency and fairness in distributed wireless networks through self-interference cancellation and scheduling. Technical report, Technical Report MSR-TR-2009-27, Microsoft Research.

Ramanathan, R., J. Redi, C. Santivanez, D. Wiggins, and S. Polit (2005). Ad hoc networking with directional antennas: a complete system solution. *Selected Areas in Communications, IEEE Journal on 23*(3), 496–506.

Schwinger, J. S., L. L. DeRaad, K. A. Milton, W.-y. Tsai, and J. Norton (1998). *Classical electrodynamics*. Perseus Books Reading, MA.

Shannon, C. E. (2001). A mathematical theory of communication. *ACM SIGMOBILE Mobile Computing and Communications Review 5*(1), 3–55.

Sousa, E. S. and J. A. Silvester (1990). Optimum transmission ranges in a direct-sequence spread-spectrum multihop packet radio network. *Selected Areas in Communications, IEEE Journal on 8*(5), 762–771.

Stoyan, D., W. S. Kendall, J. Mecke, and L. Ruschendorf (1995). *Stochastic geometry and its applications*, Volume 2. Wiley Chichester.

Tse, D. and P. Viswanath (2005). *Fundamentals of wireless communication*. Cambridge university press.

Wang, X. and H. Huang (2014). Interference and transmission capacity of full duplex wireless networks. *Submitted to IEEE JSAC Special Issue on Full-duplex Wireless Communications and Networks*.

Weber, S. P., X. Yang, J. G. Andrews, and G. De Veciana (2005). Transmission capacity of wireless ad hoc networks with outage constraints. *Information Theory, IEEE Transactions on 51*(12), 4091–4102.

Win, M. Z., P. C. Pinto, and L. A. Shepp (2009). A mathematical theory of network interference and its applications. *Proceedings of the IEEE 97*(2), 205–230.

Wyner, A. D. (1994). Shannon-theoretic approach to a gaussian cellular multiple-access channel. *Information Theory, IEEE Transactions on 40*(6), 1713–1727.

Xu, J., J. Zhang, and J. G. Andrews (2011). On the accuracy of the wyner model in cellular networks. *Wireless Communications, IEEE Transactions on 10*(9), 3098–3109.